Cell Reports

Article

MAPS integrates regulation of actin-targeting effector SteC into the virulence control network of *Salmonella* small RNA PinT

Graphical Abstract

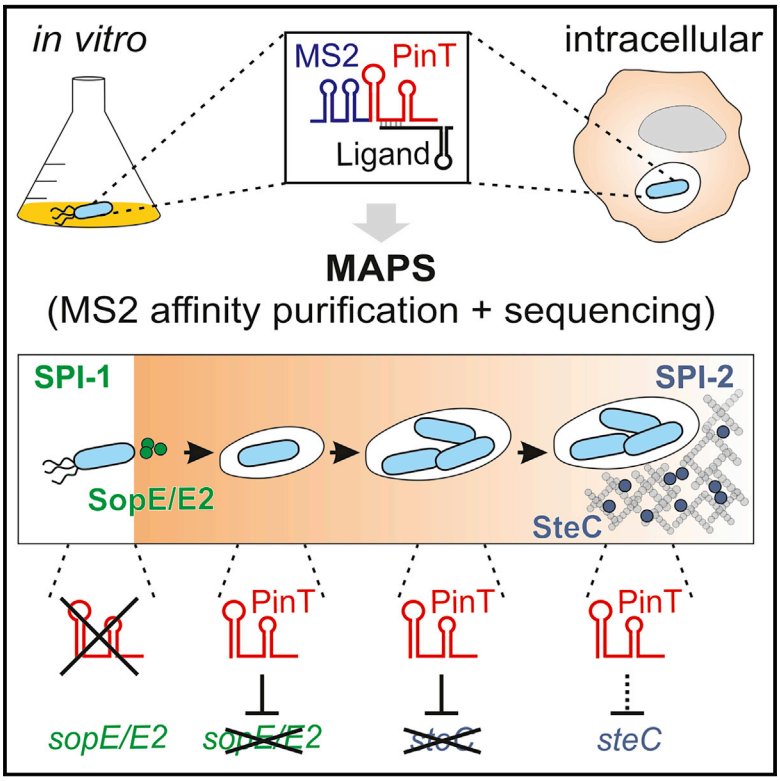

Highlights

- Advancement of MS2 affinity purification and RNA sequencing (MAPS) for bacterial sRNAs
- MAPS with physiological PinT levels on intracellular *Salmonella* reveals targets
- Translational repression of *steC* impacts host actin rearrangement during infection
- PinT is an RNA timer for the transition from SPI-1 to SPI-2 virulence programs

Authors

Sara Correia Santos, Thorsten Bischler, Alexander J. Westermann, Jörg Vogel

Correspondence

alexander.westermann@uni-wuerzburg.de (A.J.W.), joerg.vogel@uni-wuerzburg.de (J.V.)

In Brief

Correia Santos et al. use advanced affinity purification approaches to identify target candidates of *Salmonella* sRNA PinT under infection-related conditions. One of the targets identified is the mRNA of the secreted SPI-2 effector SteC, whose translation is repressed by PinT with consequences for the host cytoskeleton of infected cells.

Correia Santos et al., 2021, Cell Reports *34*, 108722
February 2, 2021
https://doi.org/10.1016/j.celrep.2021.108722

CellPress

Cell Reports

CellPress
OPEN ACCESS

Article

MAPS integrates regulation of actin-targeting effector SteC into the virulence control network of *Salmonella* small RNA PinT

Sara Correia Santos,[1] Thorsten Bischler,[2] Alexander J. Westermann,[1,3,*] and Jörg Vogel[1,3,4,*]
[1]Institute for Molecular Infection Biology, University of Würzburg, Würzburg, Germany
[2]Core Unit Systems Medicine, University of Würzburg, Würzburg, Germany
[3]Helmholtz Institute for RNA-Based Infection Research, Helmholtz Centre for Infection Research, Würzburg, Germany
[4]Lead contact
*Correspondence: alexander.westermann@uni-wuerzburg.de (A.J.W.), joerg.vogel@uni-wuerzburg.de (J.V.)
https://doi.org/10.1016/j.celrep.2021.108722

SUMMARY

A full understanding of the contribution of small RNAs (sRNAs) to bacterial virulence demands knowledge of their target suites under infection-relevant conditions. Here, we take an integrative approach to capturing targets of the Hfq-associated sRNA PinT, a known post-transcriptional timer of the two major virulence programs of *Salmonella enterica.* Using MS2 affinity purification and RNA sequencing (MAPS), we identify PinT ligands in bacteria under *in vitro* conditions mimicking specific stages of the infection cycle and in bacteria growing inside macrophages. This reveals PinT-mediated translational inhibition of the secreted effector kinase SteC, which had gone unnoticed in previous target searches. Using genetic, biochemical, and microscopic assays, we provide evidence for PinT-mediated repression of *steC* mRNA, eventually delaying actin rearrangements in infected host cells. Our findings support the role of PinT as a central post-transcriptional regulator in *Salmonella* virulence and illustrate the need for complementary methods to reveal the full target suites of sRNAs.

INTRODUCTION

To successfully initiate and sustain an infection, bacterial pathogens possess complex regulatory networks enabling them to precisely time the synthesis of their virulence proteins. Timing is crucial: if expressed too early, virulence factors and their export machineries add a substantial metabolic cost and the risk of premature sensing of a pathogen by the host. If expressed too late, the pathogen might fail to establish its protective niche in time, risking clearance by host defense mechanisms. Much of this control takes place at the DNA level, and responsible transcriptional regulators are now known for many pathogens (Cabezas et al., 2018; Colgan et al., 2016; Ellermeier and Slauch, 2007; Pérez-Morales et al., 2017; Smith et al., 2016). Starting with pioneering work on RNAIII in *Staphylococcus aureus*, bacteria have also increasingly been shown to use regulatory RNAs to integrate virulence factor production with quorum sensing, biofilm formation, and nutrient status (Guillet et al., 2013). Nonetheless, although bacterial pathogens have been shown to express many small RNAs (sRNAs) during infection (Westermann, 2018), the roles of noncoding RNA in timing virulence programs remain little understood.

In Gram-negative pathogens, evidence for sRNA control of virulence has been two-fold. First, genetic inactivation of the two major sRNA-binding proteins that facilitate sRNA-mediated regulation of mRNAs, Hfq and ProQ, typically attenuates infectivity of many species (Ansong et al., 2009; Chao and Vogel, 2010; Sittka et al., 2007; Westermann et al., 2019). Second, over the years, several mRNAs of virulence-associated proteins were identified as sRNA targets in diverse Gram-negative pathogens (Bradley et al., 2011; Gong et al., 2011; Murphy and Payne, 2007; Padalon-Brauch et al., 2008; Sievers et al., 2014), including transcripts related to virulence-associated processes such as quorum sensing and biofilm formation (Bardill et al., 2011; Lenz et al., 2004; Papenfort et al., 2015; Shao and Bassler, 2014; Sonnleitner et al., 2011).

Working in the model species *Salmonella enterica* serovar Typhimurium (henceforth, *Salmonella*), we recently identified an ~80-nt sRNA called PinT, which similarly to *S. aureus* RNAIII, seems to play a central role in timing virulence factor expression of this intracellular pathogen (Westermann et al., 2016). PinT is the top-induced noncoding transcript after *Salmonella* enters eukaryotic host cells (Westermann et al., 2016). Controlled by the PhoP/Q two-component system, this sRNA is co-activated with the physically unlinked *Salmonella* pathogenicity island 2 (SPI-2) that encodes a type III secretion system (T3SS) apparatus and corresponding effector proteins required for intracellular survival.

Three major functions of PinT have been established. First, by Hfq-dependent seed pairing, PinT downregulates specific virulence factor mRNAs (*sopE*, *sopE2*) from the SPI-1 invasion gene program (Westermann et al., 2016). Second, PinT also

inhibits invasion gene expression globally, by repressing the mRNAs of two major SPI-1 transcription factors, HilA and RtsA (Kim et al., 2019). Third, while hastening the shutoff of SPI-1, PinT delays full activation of SPI-2, by inhibiting the synthesis of the general transcription factor CRP and of the SPI-2-encoded transcriptional regulator SsrB (Kim et al., 2019; Westermann et al., 2016). In other words, PinT acts as a post-transcriptional timer, shaping the transition from one (SPI-1, invasion) to the other (SPI-2, intracellular lifestyle) major virulence program of *Salmonella*. The combined activities of PinT in *Salmonella* have a pervasive molecular effect on host cells, with ~10% of all host mRNAs showing altered expression when infected with Δ*pinT* versus wild-type bacteria (Westermann et al., 2016). Yet, PinT shares with many other sRNAs the limitation that a knockout produces no robust macroscopic phenotype in standard cell culture or mouse models (Barquist et al., 2016; Westermann et al., 2016). Therefore, to understand the full scope of PinT activity, a comprehensive analysis of its mRNA targets is needed.

Thus far, PinT targets have been predicted by pulse overexpression of the sRNA and scoring global changes in mRNA levels (Westermann et al., 2016), or by educated guesses combined with *in silico* predictions of base complementarity (Kim et al., 2019). These routes have clear limitations, e.g., sRNA pulse expression misses mRNA targets regulated only on the level of translation, but not transcript stability. Therefore, for a comprehensive view of PinT targets and mechanisms, we here apply an orthogonal approach called MS2 affinity purification and RNA sequencing (MAPS) (Lalaouna et al., 2015), which captures physical sRNA-RNA interactions in bacterial cells. In MAPS, an sRNA of interest is typically fused to an MS2 aptamer to enable recovery from cell lysates by affinity chromatography (Said et al., 2009), followed by RNA-seq analysis of co-purifying transcripts. Originally developed for the iron-responsive RyhB sRNA in *Escherichia coli* (Lalaouna et al., 2015), MAPS has since uncovered many unrecognized targets of other well-characterized *E. coli* sRNAs (Lalaouna et al., 2018, 2019b) and enabled global target screens in other bacterial species (Georg et al., 2020; Lalaouna et al., 2019a; Silva et al., 2019; Tien et al., 2018; Tomasini et al., 2017).

While these previous studies often monitored a single experimental condition and overexpressed the sRNA of interest to high levels, we here take an integrative MAPS approach under *bona fide* infection conditions, including bacterial growth inside macrophages, and seek to capture PinT targets at physiological concentrations of the sRNA (Figure 1A). This multi-condition analysis predicts a previously unrecognized PinT-mediated translational repression of the secreted SPI-2 effector SteC. Physiologically, this adds regulation of effector-induced actin rearrangement in epithelial cells to the intracellular activities of PinT. The integrative MAPS approach reported here should facilitate bottom-up analysis of sRNA targets during the intracellular phase of other bacterial pathogens.

RESULTS

Establishing MAPS for *Salmonella* PinT sRNA

MAPS requires an sRNA to tolerate fusion to a relatively large aptamer without compromising its intracellular stability, RBP association (if applicable), or base-pairing activity (Lalaouna et al., 2017). Adding a 48-nt MS2 aptamer to the 5′ end of PinT (81 nt) generates a 129-nt RNA fusion with no predicted distortion of the folding of the linked PinT (Figure 1B). To validate its functionality in *Salmonella*, we first expressed the MS2-PinT fusion from an arabinose-inducible, plasmid-borne promoter. Following induction for 10 min in early stationary phase (optical density 600 [OD_{600}] of 2.0), the MS2-PinT construct yielded the same amount of sRNA compared with an analogous expression vector harboring wild-type PinT (Figure 1C). Importantly, the MS2-PinT sRNA accumulated as a single species, i.e., the aptamer did not cause aberrant processing. Similar results were obtained with the MS2 sequence directly inserted into a plasmid-borne *pinT* gene under its native promoter, proving that the insertion did not compromise endogenous transcription of *pinT* (Figure 1D). Finally, we evaluated whether the MS2-PinT sRNA was functional, testing its ability to repress the well-characterized *sopE* mRNA target (Westermann et al., 2016). Using a *sopE::gfp* gene fusion as readout, we observed equal repression by wild-type PinT and the MS2 fusion (Figure 1F). Together, these experiments showed that the aptamer impacted neither Hfq association nor target pairing, qualifying the MS2-PinT fusion for MAPS-based target capture in *Salmonella*.

MAPS recapitulates major PinT targets and identifies new candidates

To establish MAPS-based target capture for PinT, we first performed the original MAPS protocol in *in vitro* cultures of *Salmonella*. Three different plasmids were used: the control plasmids pBAD-PinT and pBAD-MS2, expressing the untagged sRNA or the aptamer alone, respectively, and pBAD-MS2-PinT carrying the arabinose-inducible fusion sRNA. We induced these plasmids in Luria broth (LB) cultures grown to an OD_{600} of 2.0, which is a condition when SPI-1 is activated, while the endogenous PinT sRNA exhibits intermediate expression (Westermann et al., 2016). Because overexpressed PinT was known to rapidly induce target mRNA degradation, we optimized the induction time (Figure S1A). We settled on 2 min, when PinT is already abundant and the *sopE* and *sopE2* mRNAs—two well-characterized targets (Westermann et al., 2016)—start decaying.

To rank putative targets recovered with the MS2-PinT sRNA from *Salmonella* lysates, we calculated fold-enrichment comparing normalized read counts from RNA-seq of the MS2-PinT and the untagged PinT samples, each collected in duplicates (Figure 2A; Table S1, MAPS in SPI-1 conditions). Known PinT targets (*sopE*, *sopE2*, *grxA*, *crp*, *hilA*, *rtsA*, and *ssrB*) were enriched in the MS2-PinT pull-down, compared with PinT alone, confirming that the fusion sRNA was functional (Figure 2A). Surprisingly, one of the most enriched transcripts was *steC* (rank#4: SL1344_1628/*steC* 5′ UTR; Table S1, MAPS in SPI-1 conditions), a virulence factor-encoding mRNA that had gone unnoticed in all previous PinT target searches, and to which we discuss further below.

MAPS at physiological sRNA concentrations, inside host cells

All MAPS studies so far have relied upon overexpressed MS2 fusions to reach sufficiently high levels for target pull-down.

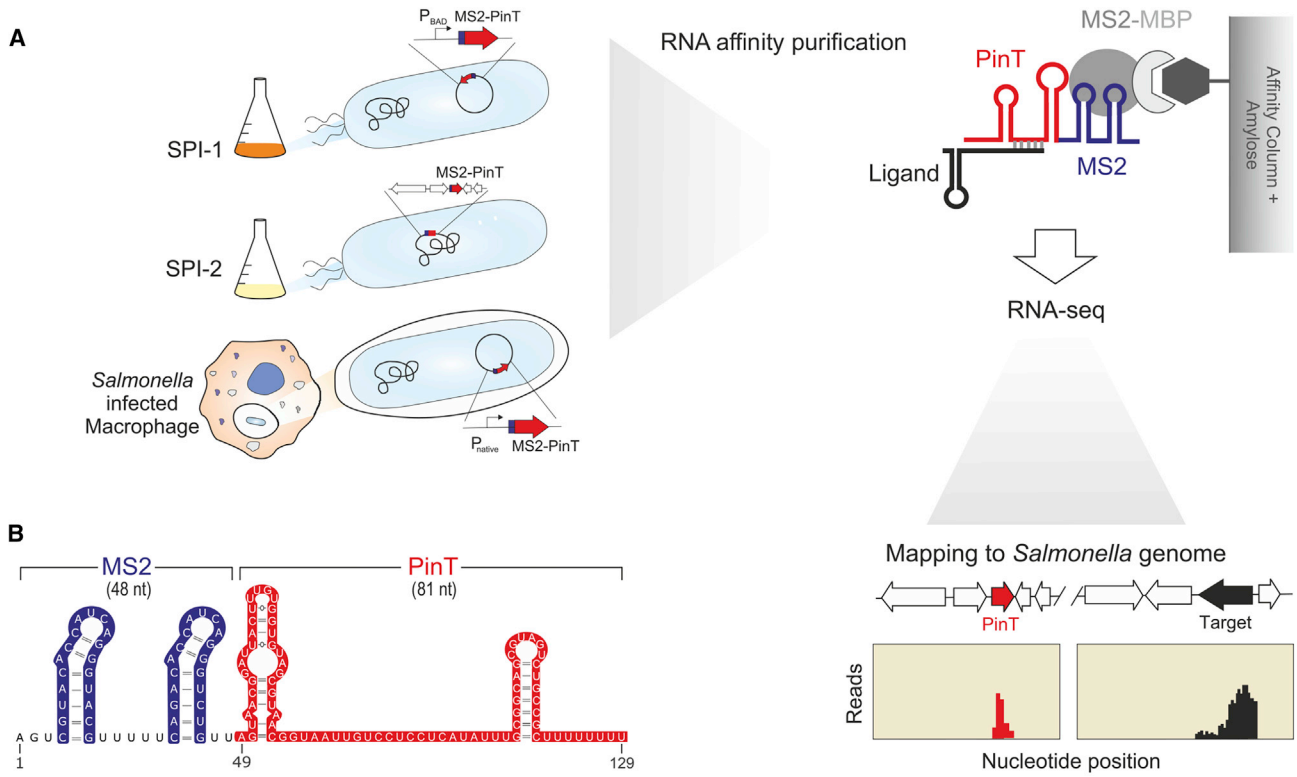

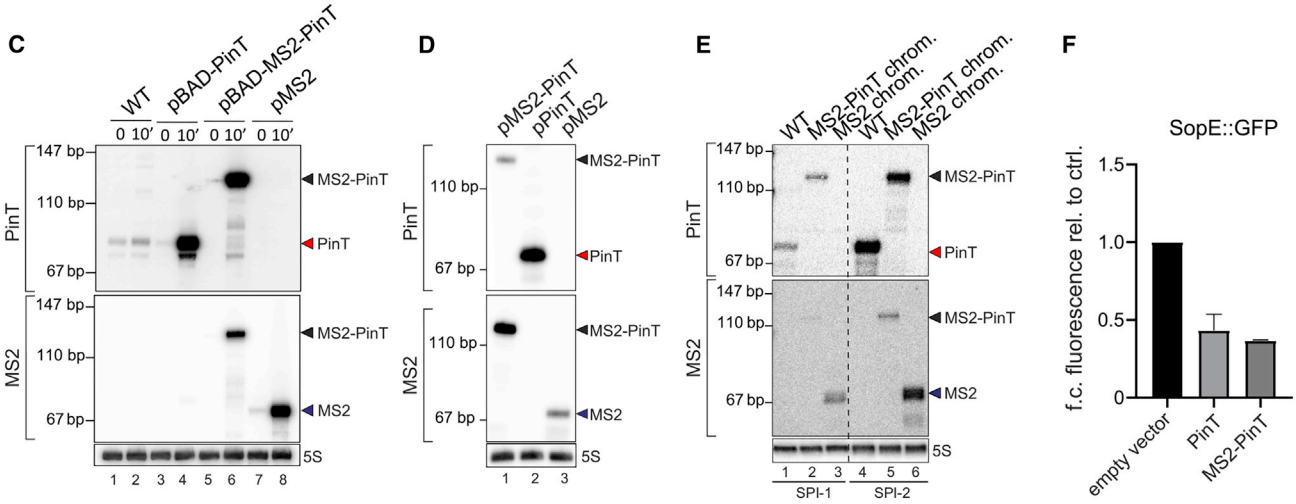

Figure 1. Establishment of MAPS for *Salmonella* PinT

(A) Overview of the different MAPS experiments performed in this study.

(B) Secondary structure prediction of MS2-PinT using the Mfold web server and VARNA applet for visualization.

(C) Northern blot analysis of *Salmonella* Typhimurium SL1344 wild-type carrying empty vector control (lanes 1 and 2, pKP8-35; JVS-1940), or the *pinT* deletion strain carrying a plasmid expressing wild-type PinT (lanes 3 and 4, pYC5-34; SCS-002), the aptamer-tagged PinT (lanes 5 and 6, pYC310; SCS-001), or the tag alone (lanes 7 and 8, pYC310; SCS-039) from an arabinose-inducible promoter, before or 10 min after induction.

(D) Northern blot of the *pinT* deletion strain carrying a plasmid with either the MS2-tagged PinT (lane 1, pSS31), untagged PinT (lane 2, pYC55), or the MS2 aptamer alone (lane 3, pSS32) under the control of the native *pinT* promoter.

(E) Northern blot analysis of *Salmonella* wild-type (lanes 1 and 4) or *Salmonella* carrying a chromosomal copy of either MS2-PinT (lanes 2 and 5) or of MS2 (lanes 3 and 6) grown under SPI-1- or SPI-2-inducing conditions. 5S rRNA serves as loading control.

(F) GFP reporter assay confirms the repression of this *bona fide* PinT target by the MS2-tagged sRNA version. In the *sopE::gfp* reporter, the complete 5′ UTR and the first 60 codons of *sopE* were fused to the GFP open reading frame. Results correspond to the mean and standard deviation of three biological replicates.

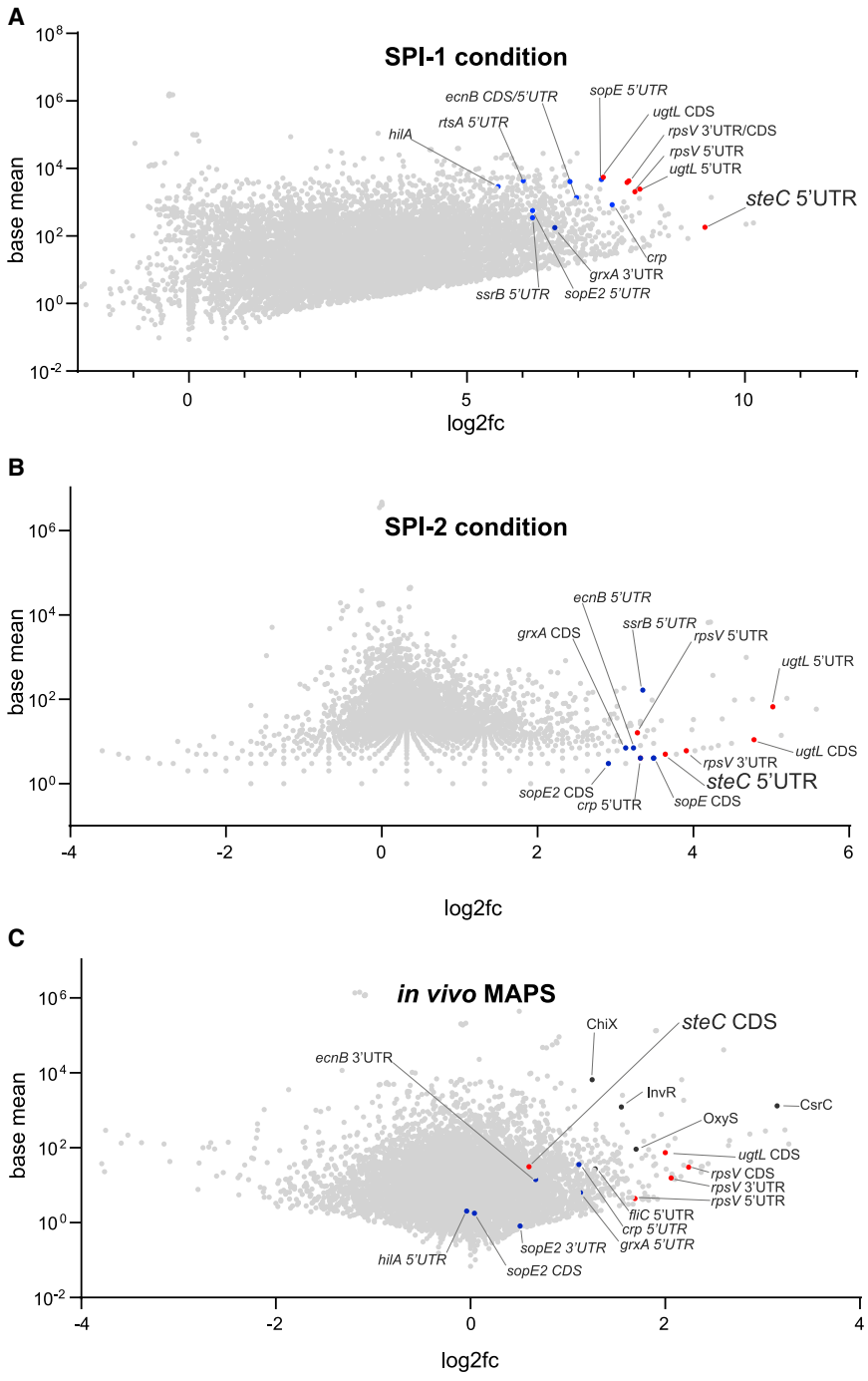

Figure 2. MAPS-derived target candidates of PinT under infection-related conditions

(A–C) MAPS under the SPI-1 condition (A), the SPI-2 condition (B), or inside mouse macrophages (C). Dots refer to individual sub-features of transcripts co-purified with PinT and are plotted according to their $\log_2$ fold-change in enrichment in the MS2-PinT relative to the untagged PinT libraries and their base mean across all sequenced libraries (as a measure of basal abundance). Data were merged over two biological replicates (except for B, where only one measurement per sample type was available). New high-confidence PinT mRNA target candidates are labeled in red and previously known ones are labeled in blue, whereas co-purified sRNAs are labeled in black. All other transcripts detected are shown in light gray. Note that the scale of the axes differs between the individual panels of this figure. In the macrophage infection model used in (C), we did not observe any major effects on infection or intracellular replication rates associated with the deletion of *pinT* or *steC*.
See also Figure S2.

However, we reasoned that the high abundance of native PinT under infection conditions (Westermann et al., 2016) would allow for MAPS under native conditions. To test this, we performed MAPS with a *Salmonella* strain in which the MS2 tag had been engineered into the chromosomal *pinT* locus (Figure 1A). Grown in a minimal medium that mimics the intracellular environment of host cells (Löber et al., 2006), this strain produced comparable levels of PinT as the wild-type strain (Figure 1E). MAPS under this condition again captured previously described targets of PinT as well as the above-identified candidate *steC* (Figure 2B; Table S1, MAPS in SPI-2 conditions).

To identify PinT targets in a true infection setting, we performed MAPS after host cell invasion, on bacteria replicating inside macrophages. In this setting, to overcome sensitivity issues resulting from the limited number of intracellular bacteria that can be recovered from infected cells, we introduced plasmids expressing MS2-PinT, untagged PinT, or the MS2 tag from the native *pinT* promoter (Figure 1A). Importantly, plasmid-borne MS2-PinT under the control of the native *pinT* promoter (rather than from an arabinose-inducible promoter) ensures that intracellular PinT kinetics mimic the endogenous sRNA expression profile, albeit producing more sRNA. Using a multiplicity of infection (MOI) of 50, ~6% of macrophages contained intracellular *Salmonella* at 4 h post-infection (p.i.). Macrophages were lysed and the recovered bacteria were subjected to MAPS. Of the ~30 million cDNA reads obtained per library, 5%–46% mapped to the eukaryotic host transcriptome and were not further considered. The majority of the *Salmonella*-specific reads were from rRNA, yet leaving 3%–18% of reads from other RNA classes for the identification of PinT targets.

Intracellular targets of PinT were predicted by calculating enrichment in MS2-PinT over the untagged PinT control (Figure 2C; Table S1). Of known targets, *grxA* and *crp* were slightly enriched with the MS2-PinT ($\log_2$ fold-change of 1.13 and 1.11,

respectively). The remaining targets, *sopE*, *sopE2*, *hilA*, *rtsA*, and *ssrB*, are underrepresented in the MS2-PinT pull-down samples ($\log_2$ fold-change $\leq$ 1), as expected since these genes are expressed earlier during infection. In other words, MAPS at this 4 h p.i. time point *in vivo* differs from the *in vitro* SPI-2 condition. Other enriched mRNAs of interest included *ugtL* encoding a membrane protein involved in PhoQ activation, *rpsV* encoding the 30S ribosomal subunit protein S22, and *fliC* encoding for the major flagellin (Figure 2C; Table S1, in vivo MAPS). As with bacteria from SPI-2 media, this MAPS experiment on intracellular bacteria again recovered the *steC* mRNA, although the enrichment was not as strong as under pre-infection conditions ($\log_2$ fold-change of 0.60 inside macrophages versus 9.28 at OD_{600} of 2.0).

PinT regulates *steC* on the post-transcriptional level

Coincidentally, we had previously used the *steC* promoter as a readout for PinT activity on CRP, assuming that this sRNA regulated the *steC* gene indirectly as part of its global effect on SPI-2 activation (Westermann et al., 2016). However, the integrated MAPS data now suggested that PinT also regulates *steC* directly, through an RNA-RNA interaction. SteC is an effector kinase secreted through the T3SS of SPI-2 into the host cytosol, where it induces the assembly of an F-actin meshwork around the *Salmonella*-containing vacuole (SCV), thereby restraining bacterial growth (Odendall et al., 2012; Poh et al., 2008). Therefore, we subsequently focused on the characterization of PinT-mediated SteC regulation and its impact on host cells during infection. To test the predicted direct regulation by PinT, we determined changes of *steC* mRNA levels after induced expression of PinT (Figure 3A). We observed a decrease in *steC* mRNA levels 20 min after sRNA induction, disappearing to roughly the same extent as the established direct target *sopE* (Figure 3A). In addition, we constructed a *Salmonella* strain in which we fused the triple FLAG epitope to the C terminus C of the *steC* reading frame, for western blot detection of the protein. Using this *steC*::3xFLAG strain, we observed that while *pinT* deletion mildly increased protein levels, constitutive PinT expression fully depleted the SteC protein (Figure 3B).

Hfq-associated sRNAs such as PinT typically repress mRNAs by antisense sequestration of the translation initiation region (Hör et al., 2020). Using *in silico* analysis for base-pairing regions, we predicted that PinT uses an extended version of its previously determined seed sequence (Westermann et al., 2016) to form an ~17-bp duplex with the Shine-Dalgarno (SD) sequence and AUG start codon of *steC* (Figure 3C; Figure S3A). Testing the presumed inhibition, we found that PinT indeed repressed a *steC*::*gfp* translational fusion, which includes the 30-nt 5′ untranslated region (5′ UTR) and the first 21 codons of *steC* (Figure 3D). Importantly, since this fusion is transcribed from a constitutive promoter, repression must occur post-transcriptionally (Figure 3D).

Using *in-vitro*-synthesized PinT sRNA and a 5′ fragment of *steC* mRNA, we observed that they readily formed a complex when incubated with each other, as shown by the electrophoretic mobility shift assay (EMSA) (Figures S3B and S3C). Binding occurred with an apparent dissociation constant (K_D) of 533 nM (Figure S3E), similar to other established sRNA-mRNA interactions without addition of Hfq (Bobrovskyy et al., 2019). When Hfq was added to the binding reaction, a further shift occurred, predicting the formation of a super complex of the two RNA partners together with Hfq (Figures S3D and S3E).

Next, we used structure probing to experimentally define the putative PinT-*steC* RNA duplex. A fixed amount of an *in-vitro*-transcribed, radiolabeled segment of *steC* mRNA (encompassing the 5′ UTR and the first 21 codons) was treated with lead(II) acetate, RNase T1, or Shortcut RNase III, without or with increasing concentrations of PinT. Visualization of the resulting cleavage products in a denaturing gel supported the *in silico* prediction that the *steC* start codon is sequestered as a result of pairing with PinT (Figure 3E).

The *in vitro* probing results allowed us to select critical bases to mutate in PinT and *steC*, finally proving a direct RNA interaction *in vivo*. Specifically, we generated a *steC*$^{\#}$*::gfp* fusion with five bases mutated in the region upstream of the start codon (Figure 3C); these changes fully abrogated repression by PinT (Figure 3D). However, compensatory changes in the sRNA (PinT$^{\#}$ variant) fully restored repression of the *steC*$^{\#}$*::gfp* fusion. Conversely, PinT$^{\#}$ also repressed the wild-type *steC::gfp* reporter, albeit less strongly than did wild-type PinT, maybe as a combined effect of PinT$^{\#}$ overexpression and the potential for seven nucleotides to form base pairs even in the mutated sRNA. Of note, although one of the point mutations introduced to generate *steC*$^{\#}$ (G→C at position −13; Figure 3C) affects the predicted SD sequence, we observed only a slight reduction of SteC synthesis (Figure S4).

Evidence for translational repression of SteC by PinT

The location of the PinT target site within *steC* 5′ UTR pointed to a direct inhibition of translation initiation. We obtained evidence for this mechanism in two different types of *in vitro* assays. First, we translated the *steC::*3xFLAG mRNA using 70S ribosomes, in the absence or presence of PinT or Hfq (Figure 4A). We observed clear inhibition of SteC::3xFLAG protein synthesis by increasing concentrations of PinT, provided Hfq was added to the reaction (Figure 4A, lanes 9 and 10). By contrast, PinT or Hfq alone did not inhibit *steC::*3xFLAG mRNA translation (lanes 3, 4, and 7). As expected, translation of the unrelated *hupA::*3xFLAG mRNA, used as a negative control, was unaltered by PinT or Hfq (lanes 5, 6, 8, 11, and 12).

Second, to prove that PinT inhibited the initiation step of translation, we performed 30S ribosome toeprinting assays (Hartz et al., 1988). The *steC::gfp* mRNA was annealed to an end-labeled primer, complementary to the *gfp* coding region, and incubated with 30S subunits in the presence or absence of uncharged tRNA^{fMet}, followed by reverse transcription. Analysis of the extension products revealed one ribosome-induced, tRNA^{fMet}-dependent toeprint at the characteristic +15-nt position (Figure 4B, lane 3). This toeprint signal strongly decreased in the presence of both PinT and Hfq (Figure 4B, lanes 6 and 7). Addition of Hfq alone, which has been reported to suffice for repression of some mRNAs (Chen and Gottesman, 2017; Ellis et al., 2017; Sonnleitner and Bläsi, 2014), did not affect the *steC* toeprint (Figure 4B, lane 8). Taken together, these results strongly support a mechanistic model whereby Hfq-dependent annealing of the PinT sRNA to this mRNA blocks the synthesis of the SPI-2-encoded effector SteC.

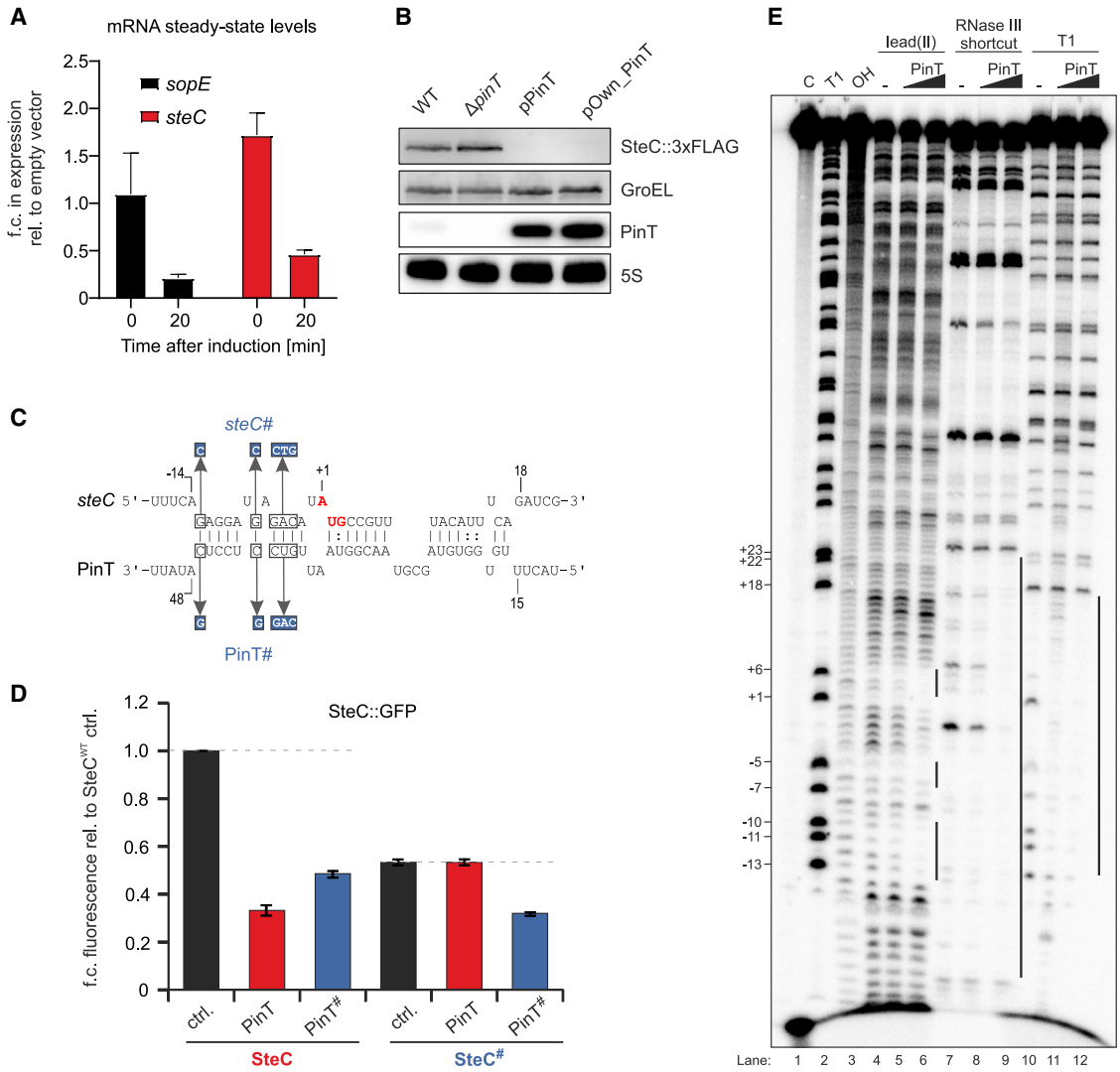

Figure 3. The *steC* mRNA is a new PinT target

(A) qRT-PCR measurements of *sopE* and *steC* mRNAs before and 20 min after pulse expression of PinT. Transcript levels are relative to strains harboring the empty vector, before or after induction, respectively. Results correspond to the mean and standard deviation of three biological replicates.

(B) Combined northern and western blot analysis of strains expressing an epitope-tagged version of SteC in either the wild-type, *pinT* deletion, or complementation background. Includes GroEL and 5S as a loading control for protein and RNA, respectively.

(C) *In silico* prediction of the interaction between *steC* mRNA and PinT. The point mutations introduced to generate PinT$^{\#}$ and *steC*$^{\#}$ are shown in blue. The start codon of *steC* is highlighted in red.

(D) Fluorescence reporter assay of *steC::gfp* or *steC*$^{\#}$*::gfp* gene fusions, as in Figure 1F. The reporters encompass the full 5′ UTR and first 21 codons of SteC. Results correspond to the mean and standard deviation of three biological replicates and are relative to the SteC^{WT} (wild-type version of SteC) reporter in absence of PinT. Note that the point mutation at position –13 (see C) partially disrupts the ribosome binding site, lowering basal expression of the SteC-GFP fusion protein by ~2-fold.

(E) *In vitro* structure probing identifies PinT targeting sites within *steC* mRNA. The 5′ end-labeled *steC* mRNA (5 nM) was subjected to RNase T1, lead(II), and Shortcut RNase III cleavage in the absence (lanes 4, 7, and 10) or presence of increasing concentrations of unlabeled PinT (0.5 μM final concentration in lanes 5, 8, and 9; 5 μM final concentration in lanes 6, 9, and 12). Vertical lines indicate the *steC* regions protected by PinT in the respective cleavage reaction. G-nucleotide positions (relative to the translational start site) are indicated to the left. C, control lane with untreated *steC*; OH, alkaline ladder for *steC*; T1, RNase T1 ladder of hydrolyzed and denatured *steC*.

PinT suppresses SteC-mediated actin rearrangement in host cells

When tested in standard *in vitro* culture, deletion of *pinT* leads to only a marginal increase in SteC protein abundance (Figure 3B), which is typical for sRNA deletion mutants (Hör et al., 2020). To test *steC* regulation in a more physiological setting, we infected HeLa cells with the *Salmonella steC*::3xFLAG strain. In this setting, deletion of *pinT* does not affect intracellular replication kinetics (Westermann et al., 2016), allowing us to directly compare western blot signals between wild-type and Δ*pinT*

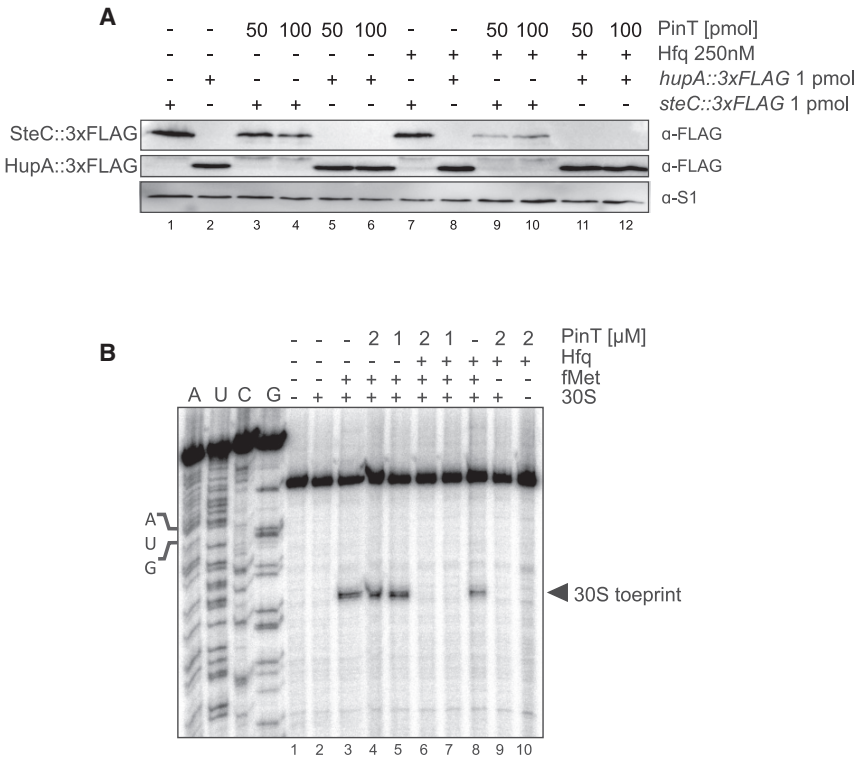

Figure 4. PinT interferes with *steC* translation initiation

(A) *In vitro* translation assay confirms that PinT interferes with initiation of *steC* translation. Full-length *steC::3xFLAG or hupA::3xFLAG* (as a negative control) mRNA fusions were *in vitro* translated with reconstituted 70S ribosomes in the presence or absence of PinT and Hfq. Ribosomal protein S1 serves as the loading control.

(B) Ribosome toeprinting assay of *steC::gfp* mRNA in presence or absence of PinT and Hfq. Nucleotide ladder is shown on the left, and the position of the 30S toeprint is indicated to the right.

infections for matched time points. We achieved to detect PinT and SteC, both expressed at physiological levels from the chromosome of intracellular *Salmonella* (Figure 5A). Intriguingly, in a time window from 6 to 12 h p.i., SteC::3xFLAG protein levels showed an ~1.5- to 2-fold elevation in the absence of PinT relative over the levels in wild-type bacteria. Thus, the PinT-mediated repression delays SteC synthesis inside host cells.

The role of SteC is best understood in non-phagocytic cells where, following its translocation from *Salmonella*, this protein primarily functions as a kinase phosphorylating a specific set of cytosolic proteins involved in host immune signaling cascades that converge at the level of actin rearrangement (Imami et al., 2013; Odendall et al., 2012; Poh et al., 2008; Walch et al., 2020). Host protein phosphorylation by SteC is thought to trigger the formation of actin bundles in the vicinity of *Salmonella* microcolonies inside host cells. Therefore, actin arrangement lent itself as a host readout for determining the potency of PinT-mediated SteC repression during infection. To this end, we performed confocal microscopy to follow actin rearrangement in Swiss 3T3 fibroblasts, in which the SPI-2-dependent F-actin phenotype is particularly well defined (Méresse et al., 2001), infected with wild-type *Salmonella*, Δ*steC* or Δ*pinT* deletion mutants, and the corresponding complementation strains expressing either *steC* or *pinT* from a pZE-*luc* plasmid or a pBAD plasmid, respectively. In addition, all strains constitutively expressed GFP to track the localization of intracellular bacteria. Infected fibroblasts were fixed 10 h p.i., and actin filaments were stained with an Alexa Fluor 595 phalloidin conjugate (Figures 5B and 5C). Uninfected bystander cells (without a GFP signal) contained very few organized actin filaments (Figure 5C). In agreement with a previous study (Poh et al., 2008), wild-type *Salmonella* caused the appearance of large clusters of condensed F-actin around the bacterial microcolonies in 97.5% of the infected cells. In case of the Δ*steC* mutant, this proportion dropped to 2% (Figures 5B and 5C). The *trans*-complementation of *steC* in the Δ*steC* background restored actin rearrangement to 90% of the infected cells.

An effect of PinT on actin rearrangement was detectable when the sRNA was overexpressed. That is, while fibroblasts infected with Δ*pinT Salmonella* displayed the same numbers of infected cells with F-actin rearrangement as for the wild-type infection (97.5%), PinT expressed from an inducible promoter on a plasmid reduced this to 22.5%. This latter reduction suggested, but did not prove, that the PinT effect on actin formation was through repression of SteC synthesis.

Next, we screened actin rearrangement in fibroblasts infected with *Salmonella* engineered to carry a *steC*$^{\#}$ allele on the chromosome (note that this allele is refractory to PinT activity; Figures 3C and 3D). One hundred percent of cells infected with this *Salmonella steC*$^{\#}$ strain presented the F-actin phenotype; in other words, the *steC*$^{\#}$ allele behaves like the wild-type *steC* gene (Figures 5B and 5C). Interestingly, even when PinT was overexpressed, expression of *steC*$^{\#}$ still resulted in actin rearrangement in 90% of the infected cells. However, the proportion of cell numbers with actin rearrangement dropped to 50% when the same *Salmonella* strain expressed PinT$^{\#}$, which harbors compensatory mutations for the *steC*$^{\#}$ sequence. Interestingly, this reduction was similar when PinT$^{\#}$ was expressed in a strain with a wild-type *steC* gene, which echoes the above-mentioned results with *gfp* reporters (Figure 3D). That is, the mutations present in PinT$^{\#}$ allow for similar repression of the *steC* and *steC*$^{\#}$ alleles. Nonetheless, the combined results support the notion that PinT, via repression of the *steC* mRNA, engages in the regulation of host actin organization during *Salmonella* infection.

DISCUSSION

Recent methodological advances enabling high-resolution transcriptome studies in the context of host infection (Hör et al.,

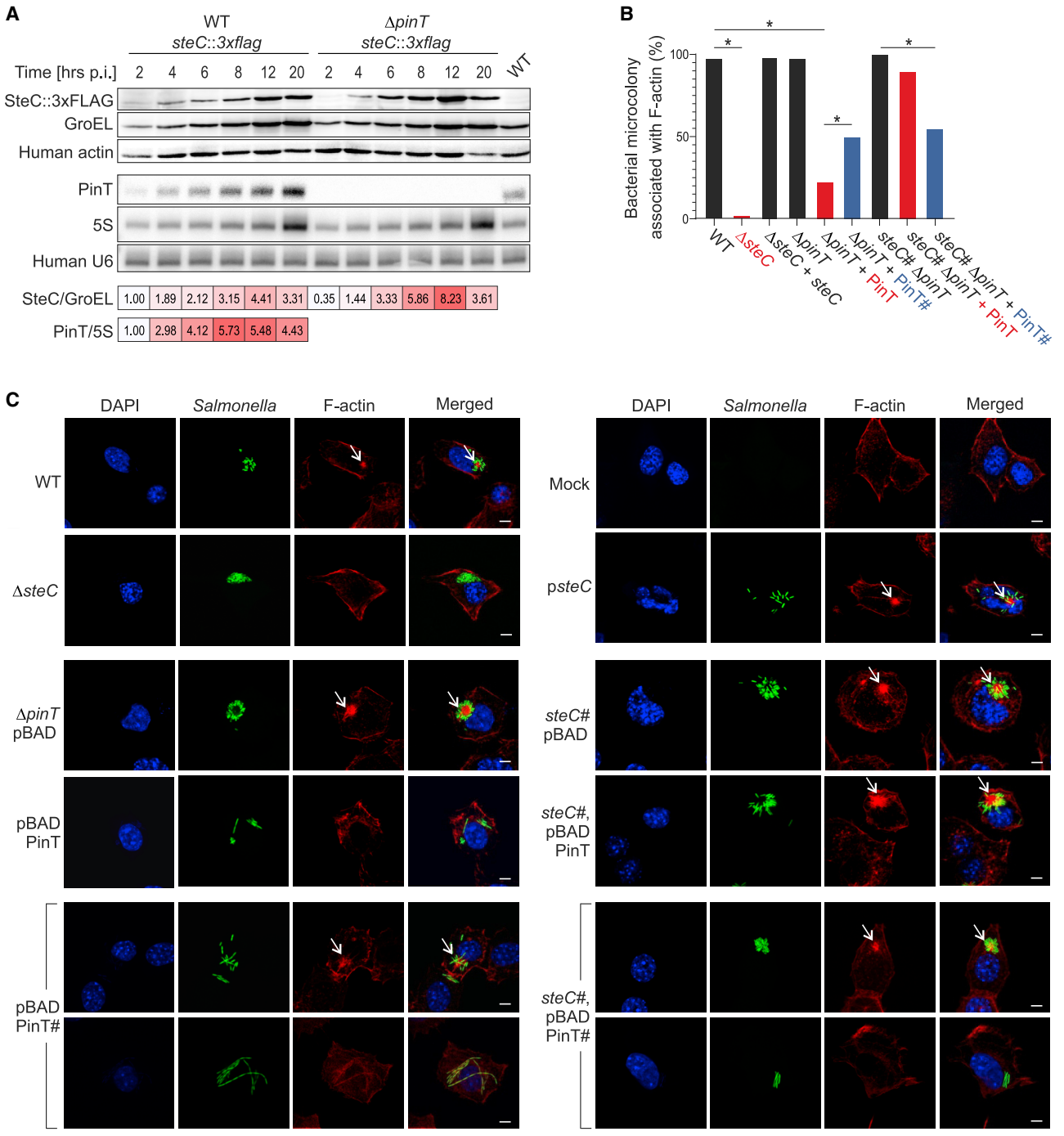

Figure 5. PinT-mediated SteC repression affects host actin rearrangement during infection

(A) Time-course expression of *Salmonella* SteC protein inside HeLa cells. Western and northern blot analyses of intracellular *Salmonella* expressing SteC::3x-FLAG in the wild-type or *pinT* deletion background. HeLa cells were infected at an MOI of 50, and total protein and RNA samples were collected at 2, 4, 6, 8, 12, and 20 h p.i. To demonstrate specificity of the SteC-FLAG signal, a 6-h sample from an infection with wild-type *Salmonella* (expressing untagged SteC) was included. Bacterial GroEL and human β-actin serve as controls for protein and *Salmonella* 5S rRNA and the human spliceosomal RNA U6 serve as controls for RNA levels, respectively. Images are representative for two biological replicates.

(B) Quantification of host F-actin remodeling by the indicated *Salmonella* strains. Swiss 3T3 fibroblast cells were infected (MOI of 100) with constitutively GFP-expressing *Salmonella* strains in either the wild-type, *steC* mutant, *pinT* mutant, SteC complementation (expressed from a constitutive promoter), or PinT complementation (from an arabinose-inducible promoter) background. Also included are *Salmonella* strains with a PinT-resistant mutant of *steC* (*steC*$^{\#}$) with or without plasmid-borne, wild-type PinT or a PinT version with compensatory mutations (PinT$^{\#}$) expressed from an arabinose-inducible promoter. Induction of PinT

(legend continued on next page)

2018; Perez-Sepulveda and Hinton, 2018; Saliba et al., 2017; Westermann et al., 2017) have identified a plethora of sRNA genes that are co-regulated with virulence genes in bacteria (Caldelari et al., 2013; Quereda and Cossart, 2017; Svensson and Sharma, 2016; Westermann, 2018). Understanding the functions of these sRNAs in bacterial pathogenesis has been much harder for two reasons: (1) due to their short length, sRNA genes are often insufficiently covered in genomic screens for virulence factors; and (2) when investigated more systematically, individual sRNA deletions are rarely found to produce robust phenotypes in classical infection assays, despite the fact that the promoters of these sRNAs often show conservation of features recognized by transcriptional master regulators of virulence (Chao and Vogel, 2010; Westermann et al., 2016). Therefore, to understand how sRNAs contribute to the success of bacterial pathogens, a comprehensive bottom-up analysis of their molecular targets may be required. Our present findings with PinT argue that it is indeed worthwhile using different complementary methods in this endeavor.

Our MAPS-based discovery of the *steC* mRNA as a new PinT target naturally prompts the question of why it was overlooked in the two previous target searches for this sRNA. The reasons are different. One of the studies (Kim et al., 2019) made use of educated guesses, selecting candidates with expected meaningful regulation around the invasion (SPI-1) phase of the *Salmonella* infection cycle, i.e., before SteC activity is relevant. The other study (Westermann et al., 2016) used sRNA pulse expression, which in general terms has been very successful at predicting interactors of *E. coli* and *Salmonella* sRNAs (Hör et al., 2020). In that study, PinT was pulse expressed for 5 min in different media as well as in *Salmonella* replicating inside epithelial cells, which was sufficient to downregulate other targets, i.e., *sopE* or *sopE2* (Westermann et al., 2016). Intriguingly, renewed inspection of that RNA-seq data shows that *steC* was downregulated, too, but did not pass as significant in any of the conditions tested. By contrast, MAPS with MS2-PinT clearly recovers *steC* as one of the top transcripts in two of the three conditions used here (Figure 2). Particularly noteworthy is the SPI-2 MAPS experiment, which expresses the MS2-tagged sRNA from the native *pinT* locus to physiological levels. The successful enrichment of *steC* and other proven PinT targets suggests potential for reducing false positives and dropouts in MAPS experiments, by avoiding overexpression of the fusion sRNA.

We have also attempted MAPS for *Salmonella* 4 h into infection of macrophages, but the results are inconclusive such that most known PinT targets do not rank among the top. In our enrichment analysis, *grxA*, *sopE*, *steC*, and *sopE2* occupy ranks #222, #316, #980, and #1,226, out of the listed 9,879 features. While the possibility remains that the macrophage experiment enriches targets whose regulation is particularly relevant as *Salmonella* resides in this particular eukaryotic cell type and time of infection, these numbers rather suggest that intracellular MAPS needs to be further improved. Improvement might come from a more rigorous depletion of contaminating eukaryotic RNA in the lysate, from the inclusion of an RNA-RNA cross-linking step, or from switching to other aptamers such as PP7 (Lim and Peabody, 2002; Tien et al., 2018) or Csy4 (Haurwitz et al., 2010; Lee et al., 2013) as sRNA fusion partners. Another possibility to increase sensitivity might be to combine MAPS with features of recent global RNA:RNA interactome techniques such as CLASH (cross-linking, ligation, and sequencing of hybrids), GRIL-seq (global small noncoding RNA target identification by ligation and sequencing), or RIL-seq (RNA interaction by ligation and sequencing) (Han et al., 2017; Melamed et al., 2016, 2018; Waters et al., 2017), e.g., purifying targets by stepwise pull down of Hfq and the MS2-tagged sRNA.

What are the biological implications of the PinT-mediated repression of *steC* during infection? To promote its intracellular lifestyle, *Salmonella* remodels the host cytoskeleton and redirects a dense meshwork of F-actin in the vicinity of the SCV, and this process crucially hinges upon SteC (Odendall et al., 2012; Poh et al., 2008). Using different *pinT* and *steC* alleles, we have confirmed that PinT can regulate actin rearrangement in infected fibroblasts through repression of SteC protein synthesis (Figures 5B and 5C). While these experiments required overexpression of PinT, we also provide evidence for the effect of PinT on SteC levels under physiological conditions (Figure 5A). SteC protein is first detected at 4 h p.i. (Poh et al., 2008) and its levels increase over time until 20 h p.i., while PinT levels peak at 8 h (Figure 5A) (Westermann et al., 2016). We interpret this expression profile (Figure 6) to mean that PinT functions to delay the arrival of SteC in the host cytosol until *Salmonella* has properly adapted its metabolism to the SCV environment. Moreover, SteC has a mild suppressive effect on bacterial growth (Poh et al., 2008); therefore, delayed expression of this effector may be necessary to get intracellular bacterial replication going. We have previously determined intracellular replication rates of Δ*pinT Salmonella* in diverse host cell types, but did not observe significant differences compared with the wild-type in any of the human or mouse cell models tested (Westermann et al., 2016). This may be because some of the cell types lack known SteC target proteins and do not show actin rearrangement upon infection and/or due to other PinT targets in *Salmonella* compensating the expected suppressive effect on replication from *steC* de-repression. Together, the complex regulatory network, with the PhoP-induced sRNA PinT repressing PhoP-activated SteC, both directly and indirectly (Figure 6), makes the *steC* mRNA a particularly interesting PinT target, encouraging future studies of the relevance of these individual PinT-SteC-mediated changes to the host on a whole-organism level and for the outcome of infection. Such studies should also address how this repression may be counteracted, for example, through sequestration of PinT by other targets or by

expression was achieved by adding arabinose directly to the media 1 h p.i. Values correspond to the percentage of infected cells (out of each 40 analyzed cells) where F-actin was associated with the bacterial microcolony at 10 h p.i. Asterisks denote significant differences between infections ($p < 0.05$, Fisher's exact test). (C) Representative confocal images of infected fibroblasts analyzed in (B). F-actin was visualized by immunofluorescence labeling with Alexa Fluor 594 phalloidin (red). Chromosomal DNA, shown in blue, was stained with DAPI. In case of pBAD-PinT and *steC*$^{\#}$,pBAD-PinT, infection caused the actin phenotype in roughly half of the cases; thus, a representative image of either phenotype is depicted. Scale bar, 1 μm.

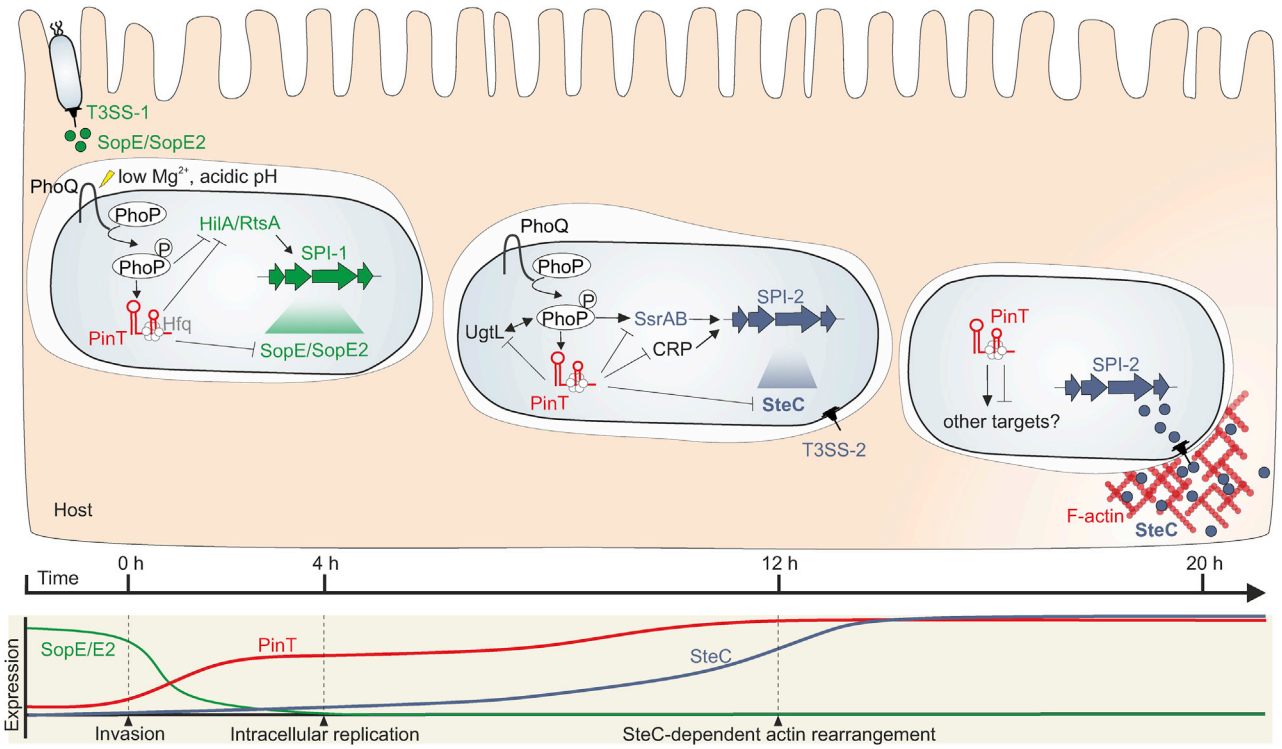

Figure 6. Model of the PinT regulatory network during infection

As shown previously (Kim et al., 2019; Westermann et al., 2016), PinT provides a post-transcriptional layer of cross-regulation between the SPI-1 and SPI-2 virulence programs. As reported here, premature expression of SteC is prevented by PinT-mediated translational interference within the first 6 h of infection. At later stages, SteC repression is alleviated through an unknown mechanism, leading to SteC synthesis, translocation, and the assembly of an F-actin meshwork around the SCV.

sRNA sponges, of which there is a growing number in bacteria (Figueroa-Bossi and Bossi, 2019).

Finally, our MAPS datasets suggest that PinT may interact with even more RNA molecules than the ones currently validated. The mRNAs for the PhoQ activator UgtL and the 30S ribosomal protein RpsV were identified in all the different pull-downs. Both *rpsV* and *ugtL* are highly upregulated in SPI-2-inducing conditions (Kröger et al., 2013) as well as inside macrophages (Srikumar et al., 2015). While we know little about the ribosomal protein RpsV, the *Salmonella*-specific inner membrane protein UgtL is known to mediate resistance to antimicrobial peptides by indirect modification of lipid A (Shi et al., 2004). UgtL is also required for gut colonization in streptomycin-treated mice (Goto et al., 2017). Most recently, UgtL was described as an activator of the PhoP/Q two-component system, contributing to *Salmonella* virulence in mice (Choi and Groisman, 2017). In other words, PinT is likely to repress the synthesis of an activator of its own transcription activator, potentially creating a feedback loop within PhoP/Q-mediated activation of SPI-2 genes (Figure 6). As such, the emerging extended target suite of PinT promises to add new examples to the growing list of intermixed regulatory loops composed of sRNAs and transcription factors, which have been studied primarily in quorum sensing, metabolic responses, and stress management as well as in the transition between motility and sessility (Beisel and Storz, 2011; Mandin et al., 2016; El Mouali et al., 2018; Shimoni et al., 2007). It will be interesting to see how the individual regulatory loops PinT is involved in affect the timing of gene expression as *Salmonella* bacteria transition through different extracellular and intracellular environments.

STAR★METHODS

Detailed methods are provided in the online version of this paper and include the following:

- KEY RESOURCES TABLE
- RESOURCE AVAILABILITY
  - Lead contact
  - Materials availability
  - Data and code availability
- EXPERIMENTAL MODEL AND SUBJECT DETAILS
  - Cell lines
  - Bacterial strains
  - Ethics Statement
- METHOD DETAILS
  - Constructing *Salmonella* mutant strains and plasmids
  - Validation of MS2-PinT expression
  - Validation of target repression by MS2-PinT
  - Northern blot

- Quantitative real-time PCR (qRT-PCR)
- GFP reporter assay
- *In vitro* MS2 affinity purification
- *Salmonella* infection assay for *in vivo* MAPS
- cDNA library preparation and sequencing
- MAPS data analysis and target selection
- Time-course pulse expression of PinT under SPI-1 and SPI-2 conditions
- Western blot
- *In vitro* structure probing and gel mobility shift assays
- *In vitro* translation assay
- Toeprinting assay
- Immunofluorescence and confocal microscopy

● QUANTIFICATION AND STATISTICAL ANALYSIS

SUPPLEMENTAL INFORMATION

Supplemental Information can be found online at https://doi.org/10.1016/j.celrep.2021.108722.

ACKNOWLEDGMENTS

We are grateful to members of the Vogel and Westermann groups, Lars Barquist, and Jay Hinton for fruitful discussions of our research and constructive comments on the manuscript. We thank Elisa Venturini, Gianluca Matera, Daniel Ryan, and Youssef El Mouali for comments on the manuscript and Yanjie Chao for help with the construction of some of the strains and plasmids used in this study. We thank David Holden's group for the 3T3 Swiss fibroblasts and for guidance with the microscopy experiments. Thanks to Barbara Plaschke, Mona Alzheimer, Sarah Reichardt, and Sandy Pernitzsch for technical support and advice. This work was supported by funds from DFG (grant Vo875-19/1 and graduate program GRK 2157/1). In addition, this work was supported by Interdisciplinary Center for Clinical Research Würzburg (grant IZKF Z-6 to T.B.).

AUTHOR CONTRIBUTIONS

Conceptualization: S.C.S., A.J.W., and J.V.; experiments: S.C.S.; bioinformatics: T.B.; supervision: A.J.W. and J.V.; funding acquisition: J.V.; writing – original draft: S.C.S., A.J.W., and J.V.; writing – review and editing: all authors.

DECLARATION OF INTERESTS

No competing interests declared.

Received: August 5, 2020
Revised: November 25, 2020
Accepted: January 13, 2021
Published: February 2, 2021

REFERENCES

Anders, S., and Huber, W. (2010). Differential expression analysis for sequence count data. Genome Biol. *11*, R106.

Ansong, C., Yoon, H., Porwollik, S., Mottaz-Brewer, H., Petritis, B.O., Jaitly, N., Adkins, J.N., McClelland, M., Heffron, F., and Smith, R.D. (2009). Global systems-level analysis of Hfq and SmpB deletion mutants in Salmonella: implications for virulence and global protein translation. PLoS ONE *4*, e4809.

Bardill, J.P., Zhao, X., and Hammer, B.K. (2011). The Vibrio cholerae quorum sensing response is mediated by Hfq-dependent sRNA/mRNA base pairing interactions. Mol. Microbiol. *80*, 1381–1394.

Barquist, L., Westermann, A.J., and Vogel, J. (2016). Molecular phenotyping of infection-associated small non-coding RNAs. Philos. Trans. R. Soc. Lond. B Biol. Sci. *371*, 20160081.

Beisel, C.L., and Storz, G. (2011). The base-pairing RNA spot 42 participates in a multioutput feedforward loop to help enact catabolite repression in Escherichia coli. Mol. Cell *41*, 286–297.

Bobrovskyy, M., Azam, M.S., Frandsen, J.K., Zhang, J., Poddar, A., Ma, X., Henkin, T.M., Ha, T., and Vanderpool, C.K. (2019). Determinants of target prioritization and regulatory hierarchy for the bacterial small RNA SgrS. Mol. Microbiol. *112*, 1199–1218.

Bradley, E.S., Bodi, K., Ismail, A.M., and Camilli, A. (2011). A genome-wide approach to discovery of small RNAs involved in regulation of virulence in Vibrio cholerae. PLoS Pathog. *7*, e1002126.

Busch, A., Richter, A.S., and Backofen, R. (2008). IntaRNA: efficient prediction of bacterial sRNA targets incorporating target site accessibility and seed regions. Bioinformatics *24*, 2849–2856.

Cabezas, C.E., Briones, A.C., Aguirre, C., Pardo-Esté, C., Castro-Severyn, J., Salinas, C.R., Baquedano, M.S., Hidalgo, A.A., Fuentes, J.A., Morales, E.H., et al. (2018). The transcription factor SlyA from Salmonella Typhimurium regulates genes in response to hydrogen peroxide and sodium hypochlorite. Res. Microbiol. *169*, 263–278.

Caldelari, I., Chao, Y., Romby, P., and Vogel, J. (2013). RNA-mediated regulation in pathogenic bacteria. Cold Spring Harb. Perspect. Med. *3*, a010298.

Chao, Y., and Vogel, J. (2010). The role of Hfq in bacterial pathogens. Curr. Opin. Microbiol. *13*, 24–33.

Chen, J., and Gottesman, S. (2017). Hfq links translation repression to stress-induced mutagenesis in *E. coli*. Genes Dev. *31*, 1382–1395.

Choi, J., and Groisman, E.A. (2017). Activation of master virulence regulator PhoP in acidic pH requires the *Salmonella*-specific protein UgtL. Sci. Signal. *10*, eaan6284.

Colgan, A.M., Kröger, C., Diard, M., Hardt, W.-D., Puente, J.L., Sivasankaran, S.K., Hokamp, K., and Hinton, J.C.D. (2016). The Impact of 18 Ancestral and Horizontally-Acquired Regulatory Proteins upon the Transcriptome and sRNA Landscape of Salmonella enterica serovar Typhimurium. PLoS Genet. *12*, e1006258.

Datsenko, K.A., and Wanner, B.L. (2000). One-step inactivation of chromosomal genes in Escherichia coli K-12 using PCR products. Proc. Natl. Acad. Sci. USA *97*, 6640–6645.

Ellermeier, J.R., and Slauch, J.M. (2007). Adaptation to the host environment: regulation of the SPI1 type III secretion system in Salmonella enterica serovar Typhimurium. Curr. Opin. Microbiol. *10*, 24–29.

Ellis, M.J., Trussler, R.S., Charles, O., and Haniford, D.B. (2017). A transposon-derived small RNA regulates gene expression in Salmonella Typhimurium. Nucleic Acids Res. *45*, 5470–5486.

El Mouali, Y., Gaviria-Cantin, T., Sánchez-Romero, M.A., Gibert, M., Westermann, A.J., Vogel, J., and Balsalobre, C. (2018). CRP-cAMP mediates silencing of Salmonella virulence at the post-transcriptional level. PLoS Genet. *14*, e1007401.

Eriksson, S., Lucchini, S., Thompson, A., Rhen, M., and Hinton, J.C.D. (2003). Unravelling the biology of macrophage infection by gene expression profiling of intracellular Salmonella enterica. Mol. Microbiol. *47*, 103–118.

Feng, J., Meyer, C.A., Wang, Q., Liu, J.S., Shirley Liu, X., and Zhang, Y. (2012). GFOLD: a generalized fold change for ranking differentially expressed genes from RNA-seq data. Bioinformatics *28*, 2782–2788.

Figueroa-Bossi, N., and Bossi, L. (2019). Sponges and Predators in the Small RNA World. In Regulating with RNA in Bacteria and Archaea, G. Storz and K. Papenfort, eds. (ASM Press), pp. 441–451.

Förstner, K.U., Vogel, J., and Sharma, C.M. (2014). READemption-a tool for the computational analysis of deep-sequencing-based transcriptome data. Bioinformatics *30*, 3421–3423.

Georg, J., Lalaouna, D., Hou, S., Lott, S.C., Caldelari, I., Marzi, S., Hess, W.R., and Romby, P. (2020). The power of cooperation: Experimental and computational approaches in the functional characterization of bacterial sRNAs. Mol. Microbiol. *113*, 603–612.

Gong, H., Vu, G.-P., Bai, Y., Chan, E., Wu, R., Yang, E., Liu, F., and Lu, S. (2011). A Salmonella small non-coding RNA facilitates bacterial invasion and

intracellular replication by modulating the expression of virulence factors. PLoS Pathog. *7*, e1002120.

Goto, R., Miki, T., Nakamura, N., Fujimoto, M., and Okada, N. (2017). Salmonella Typhimurium PagP- and UgtL-dependent resistance to antimicrobial peptides contributes to the gut colonization. PLoS ONE *12*, e0190095.

Guillet, J., Hallier, M., and Felden, B. (2013). Emerging functions for the Staphylococcus aureus RNome. PLoS Pathog. *9*, e1003767.

Han, K., Tjaden, B., and Lory, S. (2017). GRIL-seq provides a method for identifying direct targets of bacterial small regulatory RNA by in vivo proximity ligation. Nat. Microbiol. *2*, 16239.

Hartz, D., McPheeters, D.S., Traut, R., and Gold, L. (1988). Extension inhibition analysis of translation initiation complexes. Methods Enzymol. *164*, 419–425.

Haurwitz, R.E., Jinek, M., Wiedenheft, B., Zhou, K., and Doudna, J.A. (2010). Sequence- and structure-specific RNA processing by a CRISPR endonuclease. Science *329*, 1355–1358.

Hoffmann, S., Otto, C., Kurtz, S., Sharma, C.M., Khaitovich, P., Vogel, J., Stadler, P.F., and Hackermüller, J. (2009). Fast mapping of short sequences with mismatches, insertions and deletions using index structures. PLoS Comput. Biol. *5*, e1000502.

Holmqvist, E., Li, L., Bischler, T., Barquist, L., and Vogel, J. (2018). Global Maps of ProQ Binding In Vivo Reveal Target Recognition via RNA Structure and Stability Control at mRNA 3′ Ends. Mol. Cell *70*, 971–982.e6.

Hör, J., Gorski, S.A., and Vogel, J. (2018). Bacterial RNA Biology on a Genome Scale. Mol. Cell *70*, 785–799.

Hör, J., Matera, G., Vogel, J., Gottesman, S., and Storz, G. (2020). Trans-Acting Small RNAs and Their Effects on Gene Expression in *Escherichia coli* and *Salmonella enterica*. Ecosal Plus *9*. https://doi.org/10.1128/ecosalplus.ESP-0030-2019.

Imami, K., Bhavsar, A.P., Yu, H., Brown, N.F., Rogers, L.D., Finlay, B.B., and Foster, L.J. (2013). Global impact of Salmonella pathogenicity island 2-secreted effectors on the host phosphoproteome. Mol. Cell. Proteomics *12*, 1632–1643.

Kim, K., Palmer, A.D., Vanderpool, C.K., and Slauch, J.M. (2019). The small RNA PinT contributes to PhoP-mediated regulation of the SPI1 T3SS in Salmonella enterica serovar Typhimurium. J. Bacteriol. *201*, e00312.

Kröger, C., Dillon, S.C., Cameron, A.D.S., Papenfort, K., Sivasankaran, S.K., Hokamp, K., Chao, Y., Sittka, A., Hébrard, M., Händler, K., et al. (2012). The transcriptional landscape and small RNAs of Salmonella enterica serovar Typhimurium. Proc. Natl. Acad. Sci. USA *109*, E1277–E1286.

Kröger, C., Colgan, A., Srikumar, S., Händler, K., Sivasankaran, S.K., Hammarlöf, D.L., Canals, R., Grissom, J.E., Conway, T., Hokamp, K., and Hinton, J.C.D. (2013). An infection-relevant transcriptomic compendium for Salmonella enterica Serovar Typhimurium. Cell Host Microbe *14*, 683–695.

Lalaouna, D., Carrier, M.C., Semsey, S., Brouard, J.S., Wang, J., Wade, J.T., and Massé, E. (2015). A 3′ external transcribed spacer in a tRNA transcript acts as a sponge for small RNAs to prevent transcriptional noise. Mol. Cell *58*, 393–405.

Lalaouna, D., Prévost, K., Eyraud, A., and Massé, E. (2017). Identification of unknown RNA partners using MAPS. Methods *117*, 28–34.

Lalaouna, D., Prévost, K., Laliberté, G., Houé, V., and Massé, E. (2018). Contrasting silencing mechanisms of the same target mRNA by two regulatory RNAs in Escherichia coli. Nucleic Acids Res. *46*, 2600–2612.

Lalaouna, D., Baude, J., Wu, Z., Tomasini, A., Chicher, J., Marzi, S., Vandenesch, F., Romby, P., Caldelari, I., and Moreau, K. (2019a). RsaC sRNA modulates the oxidative stress response of Staphylococcus aureus during manganese starvation. Nucleic Acids Res. *47*, 9871–9887.

Lalaouna, D., Eyraud, A., Devinck, A., Prévost, K., and Massé, E. (2019b). GcvB small RNA uses two distinct seed regions to regulate an extensive targetome. Mol. Microbiol. *111*, 473–486.

Lee, H.Y., Haurwitz, R.E., Apffel, A., Zhou, K., Smart, B., Wenger, C.D., Laderman, S., Bruhn, L., and Doudna, J.A. (2013). RNA-protein analysis using a conditional CRISPR nuclease. Proc. Natl. Acad. Sci. USA *110*, 5416–5421.

Lenz, D.H., Mok, K.C., Lilley, B.N., Kulkarni, R.V., Wingreen, N.S., and Bassler, B.L. (2004). The small RNA chaperone Hfq and multiple small RNAs control quorum sensing in Vibrio harveyi and Vibrio cholerae. Cell *118*, 69–82.

Lim, F., and Peabody, D.S. (2002). RNA recognition site of PP7 coat protein. Nucleic Acids Res. *30*, 4138–4144.

Livak, K.J., and Schmittgen, T.D. (2001). Analysis of relative gene expression data using real-time quantitative PCR and the 2(-Δ Δ C(T)) Method. Methods *25*, 402–408.

Löber, S., Jäckel, D., Kaiser, N., and Hensel, M. (2006). Regulation of Salmonella pathogenicity island 2 genes by independent environmental signals. Int. J. Med. Microbiol. *296*, 435–447.

Love, M.I., Huber, W., and Anders, S. (2014). Moderated estimation of fold change and dispersion for RNA-seq data with DESeq2. Genome Biol. *15*, 550.

Mandin, P., Chareyre, S., and Barras, F. (2016). A Regulatory Circuit Composed of a Transcription Factor, IscR, and a Regulatory RNA, RyhB, Controls Fe-S Cluster Delivery. mBio. *7*, e00966-16.

Martin, M. (2011). Cutadapt removes adapter sequences from high-throughput sequencing reads. EMBnet. J. *17*, 3.

Melamed, S., Peer, A., Faigenbaum-Romm, R., Gatt, Y.E., Reiss, N., Bar, A., Altuvia, Y., Argaman, L., and Margalit, H. (2016). Global Mapping of Small RNA-Target Interactions in Bacteria. Mol. Cell *63*, 884–897.

Melamed, S., Faigenbaum-Romm, R., Peer, A., Reiss, N., Shechter, O., Bar, A., Altuvia, Y., Argaman, L., and Margalit, H. (2018). Mapping the small RNA interactome in bacteria using RIL-seq. Nat. Protoc. *13*, 1–33.

Méresse, S., Unsworth, K.E., Habermann, A., Griffiths, G., Fang, F., Martínez-Lorenzo, M.J., Waterman, S.R., Gorvel, J.P., and Holden, D.W. (2001). Remodelling of the actin cytoskeleton is essential for replication of intravacuolar Salmonella. Cell. Microbiol. *3*, 567–577.

Murphy, E.R., and Payne, S.M. (2007). RyhB, an iron-responsive small RNA molecule, regulates Shigella dysenteriae virulence. Infect. Immun. *75*, 3470–3477.

Odendall, C., Rolhion, N., Förster, A., Poh, J., Lamont, D.J., Liu, M., Freemont, P.S., Catling, A.D., and Holden, D.W. (2012). The Salmonella kinase SteC targets the MAP kinase MEK to regulate the host actin cytoskeleton. Cell Host Microbe *12*, 657–668.

Padalon-Brauch, G., Hershberg, R., Elgrably-Weiss, M., Baruch, K., Rosenshine, I., Margalit, H., and Altuvia, S. (2008). Small RNAs encoded within genetic islands of Salmonella typhimurium show host-induced expression and role in virulence. Nucleic Acids Res. *36*, 1913–1927.

Papenfort, K., Förstner, K.U., Cong, J.-P., Sharma, C.M., and Bassler, B.L. (2015). Differential RNA-seq of Vibrio cholerae identifies the VqmR small RNA as a regulator of biofilm formation. Proc. Natl. Acad. Sci. USA *112*, E766–E775.

Pérez-Morales, D., Banda, M.M., Chau, N.Y.E., Salgado, H., Martínez-Flores, I., Ibarra, J.A., Ilyas, B., Coombes, B.K., and Bustamante, V.H. (2017). The transcriptional regulator SsrB is involved in a molecular switch controlling virulence lifestyles of Salmonella. PLoS Pathog. *13*, e1006497.

Perez-Sepulveda, B.M., and Hinton, J.C.D. (2018). Functional Transcriptomics for Bacterial Gene Detectives. Microbiol. Spectr. *6*. https://doi.org/10.1128/microbiolspec.RWR-0033-2018.

Pfeiffer, V., Sittka, A., Tomer, R., Tedin, K., Brinkmann, V., and Vogel, J. (2007). A small non-coding RNA of the invasion gene island (SPI-1) represses outer membrane protein synthesis from the Salmonella core genome. Mol. Microbiol. *66*, 1174–1191.

Poh, J., Odendall, C., Spanos, A., Boyle, C., Liu, M., Freemont, P., and Holden, D.W. (2008). SteC is a Salmonella kinase required for SPI-2-dependent F-actin remodelling. Cell. Microbiol. *10*, 20–30.

Quereda, J.J., and Cossart, P. (2017). Regulating Bacterial Virulence with RNA. Annu. Rev. Microbiol. *71*, 263–280.

Said, N., Rieder, R., Hurwitz, R., Deckert, J., Urlaub, H., and Vogel, J. (2009). In vivo expression and purification of aptamer-tagged small RNA regulators. Nucleic Acids Res. *37*, e133.

Saliba, A.-E., Santos, S.C., and Vogel, J. (2017). New RNA-seq approaches for the study of bacterial pathogens. Curr. Opin. Microbiol. *35*, 78–87.

Shao, Y., and Bassler, B.L. (2014). Quorum regulatory small RNAs repress type VI secretion in Vibrio cholerae. Mol. Microbiol. *92*, 921–930.

Shi, Y., Cromie, M.J., Hsu, F.-F., Turk, J., and Groisman, E.A. (2004). PhoP-regulated Salmonella resistance to the antimicrobial peptides magainin 2 and polymyxin B. Mol. Microbiol. *53*, 229–241.

Shimoni, Y., Friedlander, G., Hetzroni, G., Niv, G., Altuvia, S., Biham, O., and Margalit, H. (2007). Regulation of gene expression by small non-coding RNAs: a quantitative view. Mol. Syst. Biol. *3*, 138.

Sievers, S., Sternkopf Lillebæk, E.M., Jacobsen, K., Lund, A., Mollerup, M.S., Nielsen, P.K., and Kallipolitis, B.H. (2014). A multicopy sRNA of *Listeria monocytogenes* regulates expression of the virulence adhesin LapB. Nucleic Acids Res. *42*, 9383–9398.

Silva, I.J., Barahona, S., Eyraud, A., Lalaouna, D., Figueroa-Bossi, N., Massé, E., and Arraiano, C.M. (2019). SraL sRNA interaction regulates the terminator by preventing premature transcription termination of *rho* mRNA. Proc. Natl. Acad. Sci. USA *116*, 3042–3051.

Sittka, A., Pfeiffer, V., Tedin, K., and Vogel, J. (2007). The RNA chaperone Hfq is essential for the virulence of Salmonella typhimurium. Mol. Microbiol. *63*, 193–217.

Smith, C., Stringer, A.M., Mao, C., Palumbo, M.J., and Wade, J.T. (2016). Mapping the Regulatory Network for Salmonella enterica Serovar Typhimurium Invasion. MBio *7*, e01024-16.

Sonnleitner, E., and Bläsi, U. (2014). Regulation of Hfq by the RNA CrcZ in Pseudomonas aeruginosa carbon catabolite repression. PLoS Genet. *10*, e1004440.

Sonnleitner, E., Gonzalez, N., Sorger-Domenigg, T., Heeb, S., Richter, A.S., Backofen, R., Williams, P., Hüttenhofer, A., Haas, D., and Bläsi, U. (2011). The small RNA PhrS stimulates synthesis of the Pseudomonas aeruginosa quinolone signal. Mol. Microbiol. *80*, 868–885.

Srikumar, S., Kröger, C., Hébrard, M., Colgan, A., Owen, S.V., Sivasankaran, S.K., Cameron, A.D.S., Hokamp, K., and Hinton, J.C.D. (2015). RNA-seq Brings New Insights to the Intra-Macrophage Transcriptome of Salmonella Typhimurium. PLoS Pathog. *11*, e1005262.

Svensson, S.L., and Sharma, C.M. (2016). Small RNAs in Bacterial Virulence and Communication. Microbiol. Spectr. *4*. https://doi.org/10.1128/microbiolspec.VMBF-0028-2015.

Tien, M., Fiebig, A., and Crosson, S. (2018). Gene network analysis identifies a central post-transcriptional regulator of cellular stress survival. eLife *7*, e33684.

Tomasini, A., Moreau, K., Chicher, J., Geissmann, T., Vandenesch, F., Romby, P., Marzi, S., and Caldelari, I. (2017). The RNA targetome of Staphylococcus aureus non-coding RNA RsaA: impact on cell surface properties and defense mechanisms. Nucleic Acids Res. *45*, 6746–6760.

Walch, P., Selkrig, J., Knodler, L.A., Rettel, M., Stein, F., Fernandez, K., Viéitez, C., Potel, C.M., Scholzen, K., Geyer, M., et al. (2020). Global mapping of Salmonella enterica-host protein-protein interactions during infection. bioRxiv. https://doi.org/10.1101/2020.05.04.075937.

Waters, S.A., McAteer, S.P., Kudla, G., Pang, I., Deshpande, N.P., Amos, T.G., Leong, K.W., Wilkins, M.R., Strugnell, R., Gally, D.L., et al. (2017). Small RNA interactome of pathogenic E. coli revealed through crosslinking of RNase E. EMBO J. *36*, 374–387.

Westermann, A.J. (2018). Regulatory RNAs in Virulence and Host-Microbe Interactions. Microbiol. Spectr. *6*. https://doi.org/10.1128/microbiolspec.RWR-0002-2017.

Westermann, A.J., and Vogel, J. (2018). Host-Pathogen Transcriptomics by Dual RNA-Seq. Methods Mol. Biol. *1737*, 59–75.

Westermann, A.J., Förstner, K.U., Amman, F., Barquist, L., Chao, Y., Schulte, L.N., Müller, L., Reinhardt, R., Stadler, P.F., and Vogel, J. (2016). Dual RNA-seq unveils noncoding RNA functions in host-pathogen interactions. Nature *529*, 496–501.

Westermann, A.J., Barquist, L., and Vogel, J. (2017). Resolving host-pathogen interactions by dual RNA-seq. PLoS Pathog. *13*, e1006033.

Westermann, A.J., Venturini, E., Sellin, M.E., Förstner, K.U., Hardt, W.-D., and Vogel, J. (2019). The Major RNA-Binding Protein ProQ Impacts Virulence Gene Expression in Salmonella enterica Serovar Typhimurium. MBio *10*, e02504-18.

Zuker, M. (2003). Mfold web server for nucleic acid folding and hybridization prediction. Nucleic Acids Res. *31*, 3406–3415.

STAR★METHODS

KEY RESOURCES TABLE

REAGENT or RESOURCE	SOURCE	IDENTIFIER
Antibodies		
anti-FLAG	Sigma-Aldrich	Sigma-Aldrich Cat# F3165, RRID:AB_259529
anti-GroEL	Sigma-Aldrich	Sigma-Aldrich Cat# G6532, RRID:AB_259939
anti-GFP	Roche Applied Science	Roche Cat# 11814460001, RRID:AB_390913
anti-actin	Sigma-Aldrich	Sigma-Aldrich Cat# A5316, RRID:AB_476743
anti-S1	M. Springer, IBPC Paris, France	n.a.
anti-mouse	GE- Healthcare	Thermo Fisher Scientific Cat# 10106134, RRID:AB_772193
anti-rabbit	Thermo Scientific	Thermo Fisher Scientific Cat# 31460, RRID:AB_228341
Bacterial and virus strains		
WT	Nature. 1981 May 21;291(5812):238-9	JVS-1574
wild-type lambda red	Vogel lab strain	JVS-3013
WT_GFP	Mol Microbiol. 2009 Oct;74(1):139-58	JVS-3858
Δ*pinT*	Nature volume 529, pages496–501(2016)	YCS-034
Δ*pinT*_GFP	Nature volume 529, pages496–501(2016)	JVS-10038
SteC3xFLAG	This paper	JVS-10980
Δ*steC* GFP	This paper	JVS-11355
Δ*pinT*, *steC*::3xFLAG	This paper	JVS-11586
Δ*pinT*, *steC*::3xFLAG PinT	This paper	JVS-11635
Δ*pinT*, *steC*::3xFLAG PinT	This paper	JVS-11638
Δ*pinT*, *steC*#..3xFLAG	This paper	JVS-12702
WT, pBAD	Mol Microbiol. 2006 Dec;62(6):1674-88	JVS-1940
Δ*pinT*, pBAD-PinT	This paper	JVS-11716
Δ*pinT*, pBAD	This paper	JVS-11717
Δ*pinT*, pBAD-PinT, GFP control	This paper	JVS-11719
Δ*pinT*, pBAD + GFP control	This paper	JVS-11721
Δ*pinT*, pBAD, *steC*::*gfp*	This paper	JVS-11727
Δ*pinT*, pBAD-PinT, *steC*::*gfp*	This paper	JVS-11728
Δ*pinT*, pown_PinT	This paper	JVS-11979
Δ*pinT*, pOWN-MS2-PinT	This paper	JVS-12092
Δ*pinT*, pOWN_MS2	This paper	JVS-12093
Chromosomal MS2-PinT	This paper	JVS-12103
c.*pinT* > MS2-Term	This paper	JVS-12247
*Δpin*T, *steC*::3xFLAG	This paper	JVS-12401
steC::3xFLAG	This paper	JVS-12407
Δ*pinT*, Ptet-GFP, *steC*6mut, pBAD	This paper	JVS-12501
Δ*pinT*, Ptet-GFP, *steC*6mut, pBAD-PinT	This paper	JVS-12503
Δ*pinT* + MS2-PinT	This paper	SCS-001
Δ*pinT* + PinT	This paper	SCS-002

(*Continued on next page*)

Continued

REAGENT or RESOURCE	SOURCE	IDENTIFIER
Δ*pinT* + MS2-PinT + *sopE*::*gfp*	This paper	SCS-003
Δ*pinT* + MS2-PinT + *sopE2*::*gfp*	This paper	SCS-004
Δ*pinT* + PinT + *sopE2*::*gfp*	This paper	SCS-005
Δ*pinT*, MS2-PinT, GFP control	This paper	SCS-007
Δ*pinT*, PinT, GFP control	This paper	SCS-008
Δ*pinT* + pBAD	This paper	SCS-013
Δ*pinT*, PinT, *sopE*::*gfp*	This paper	SCS-017
Δ*pinT*, MS2	This paper	SCS-039
Δ*pinT*, PinT#, GFP control	This paper	SCS-104
Δ*pinT*, PinT#, *steC*::*gfp*	This paper	SCS-106
Δ*pinT*, pBAD, *steC#*::*gfp*	This paper	SCS-108
Δ*pinT*, PinT, *steC#*::*gfp*	This paper	SCS-109
Δ*pinT*, PinT#, *steC#*::*gfp*	This paper	SCS-110
Δ*pinT*, GFP, pBAD-PinT#	This paper	SCS-172
Δ*pinT*, GFP, pBAD-PinT	This paper	SCS-173
Δ*pinT*, GFP, pBAD	This paper	SCS-174
Δ*pinT*, GFP, pOwn-MS2-PinT	This paper	SCS-175
Δ*pinT*, GFP, pOwn-MS2	This paper	SCS-176
Δ*pinT*, GFP, pOwn-PinT	This paper	SCS-177
Δ*pinT*, GFP, pBAD-PinT#	This paper	SCS-178
Biological samples		
Mouse serum	Sigma-Aldrich	M5905-5ML
FCS	Biochrom	S0115
Chemicals, peptides, and recombinant proteins		
TRIzol LS reagent	Invitrogen	10296028
DNase I	Fermentas	EN0521
Hybri-Quick buffer	Carl Roth AG	A981.1
amylose	New England Biolabs	#E8021S
Glycoblue	Invitrogen	AM9516
DMEM	GIBCO	D6429-24X500ML
DPBS	GIBCO	D8662-24X500ML
Western Lightning solution	Perkin Elmer	NEL122001EA
lead(II) acetate	Fluka	15623800
RNase T1	Ambion	AM2283
Shortcut RNase III	New England Biolabs	#M0245S
30S ribosomal subunit	K. Nierhaus, Max Planck Institute for Molecular Genetics, Berlin, Germany	n.a.
Alexa Fluor 594 Phalloidin	ThermoFisher	A12381
VECTASHIELD(R) Mounting Medium	Biozol	VEC-H-1000
Critical commercial assays		
Power SYBR Green RNA-to-CT 1-Step kit	Applied Biosystems	50-591-795
Agencourt AMPure XP kit	Beckman Coulter Genomics	A63881
MEGAscript T7 Kit	Invitrogen	AMB13345
PURExpress® *In Vitro* Protein Synthesis Kit	New England Biolabs	E6800S
CycleReader™ DNA Sequencing Kit	Fermentas	K1711
Deposited Data		
Raw and analyzed data	This paper	GEO: GSE157499

(*Continued on next page*)

Continued

REAGENT or RESOURCE	SOURCE	IDENTIFIER
Experimental models: cell lines		
HeLa-S3	Sigma-Aldrich	ATCC® CCL-2.2
iBMM	BEI Resources, NIAID, NIH	Macrophage cell line derived from wild type mice, NR-9456
Swiss 3T3	David Holden (Imperial College London)	ATCC® CCL-92
Oligonucleotides		
See Table S2 for oligonucleotide sequences.	This paper	n.a.
Recombinant DNA		
pBAD-ctrl.	Mol Microbiol. 2006 Dec;62(6):1674-88	pKP8-35
pKD4	Proc Natl Acad Sci U S A. 2000 Jun 6;97(12):6640-5	pKD4
pSUB11	Proc Natl Acad Sci U S A. 2001 Dec 18; 98(26): 15264–15269.	pSUB11
FLP helper plasmid	Proc Natl Acad Sci U S A. 2000 Jun 6;97(12):6640-5	pCP20
Pown-ctrl.	Nature volume 529, pages496–501(2016)	pJV300
Pown-pinT	Nature volume 529, pages496–501(2016)	pYC55
pXG-10	Nucleic Acids Res. 2007;35(3):1018-37	pXG-10
sopE::gfp	Nature volume 529, pages496–501(2016)	pYC17
sopE2::gfp	Nature volume 529, pages496–501(2016)	pYC41
pXG-0	Nucleic Acids Res. 2007;35(3):1018-37	pXG-0
pXG-1	Nucleic Acids Res. 2007;35(3):1018-37	pXG-1
pBAD-PinT	Nature volume 529, pages496–501(2016)	pYC5-34
pOWN-PinT	Nature volume 529, pages496–501(2016)	pYC55
pPinT	Nature volume 529, pages496–501(2016)	pYC11
pSTnc870	This paper	pYC128
pBAD-MS2	This paper	pYC310
pBAD-MS2PinT	This paper	pYC362
steC::gfp	This paper	pSS06
pOwn-MS2-PinT	This paper	pSS031
pOwn-MS2	This paper	pSS032
pBAD-PinT#	This paper	pSS048
pSteC#::GFP	This paper	pSS054
pSteC	This paper	pSS64
Software and algorithms		
Mfold	Zuker, 2003	www.bioinfo.rpi.edu/applications/mfold/
Cyflogic software (CyFlo)	n.a.	http://www.cyflogic.com/
ImageJ	n.a.	https://imagej.nih.gov/ij/download.html
LAS AF Lite software	n.a.	Leica
Cutadapt (v1.10/1.12/1.16/2.5)	Martin, 2011	https://cutadapt.readthedocs.io/en/stable/
READemption (v0.4.3/0.4.5)	Förstner et al., 2014	https://reademption.readthedocs.io/en/latest/
segemehl (v0.2.0)	Hoffmann et al., 2009	http://www.bioinf.uni-leipzig.de/Software/segemehl/
DESeq2 (v1.13.8/1.24.0)	Love et al., 2014	http://bioconductor.org/packages/release/bioc/html/DESeq2.html
GFOLD (v1.1.4)	Feng et al., 2012	https://zhanglab.tongji.edu.cn/softwares/GFOLD/index.html

(*Continued on next page*)

Continued

REAGENT or RESOURCE	SOURCE	IDENTIFIER
Other		
Bio-Spin disposable chromatography columns	BioRad	#732-6008
T75 flasks	Corning	CLS431080
PVDF membrane	Perkin Elmer	NEF1002001PK

RESOURCE AVAILABILITY

Lead contact

Further information and requests for resources and reagents should be directed to the Lead Contact, Jörg Vogel (joerg.vogel@uni-wuerzburg.de).

Materials availability

Primary material generated in this study will be made available upon request following publication.

Data and code availability

Sequencing data are available at NCBI Gene Expression Omnibus (https://www.ncbi.nlm.nih.gov/geo) under the accession number GSE157499 (https://www.ncbi.nlm.nih.gov/geo/query/acc.cgi?acc=GSE157499).

EXPERIMENTAL MODEL AND SUBJECT DETAILS

Cell lines

Cell lines used in this study were human epithelial HeLa-S3 (Sigma-Aldrich; ATCC® CCL-2.2), mouse macrophages iBMM (BEI Resources, NIAID, NIH, NR-9456), and mouse fibroblasts Swiss 3T3 (ATCC® CCL-92; kindly provided by David Holden, Imperial College London) and were all passaged according to the providers' guidelines.

Bacterial strains

The bacterial strains used in this study are listed in Table S2. As by default, *S. enterica* strains were cultured in LB medium at 37°C in presence of the respective selection antibiotic (where appropriate; see Table S2).

Ethics Statement

Not applicable.

METHOD DETAILS

Constructing *Salmonella* mutant strains and plasmids

The MS2 aptamer (48 nt) was fused to the 5′ end of PinT, resulting in a 129 nt-long hybrid RNA molecule (Figure 1B). Correct folding of both, MS2 and PinT was supported by *in silico* RNA secondary structure prediction using Mfold (Zuker, 2003; www.bioinfo.rpi.edu/applications/mfold/). The aptamer-sRNA fusion was introduced in the pBAD plasmid, rendering MS2-PinT expression arabinose-inducible (plasmid pYC362). To construct the MS2 control plasmid (pYC310), which expresses the MS2 tag alone, pYC128 was re-amplified using oligonucleotides JVO-13630/13632 and self-ligated. The plasmid expressing MS2-PinT from the native *pinT* promoter (pYC55) was previously reported (Westermann et al., 2016). Plasmids were introduced into *Salmonella* by electroporation as described (Pfeiffer et al., 2007).

To express MS2-PinT from the chromosome, we adapted the λ Red recombinase method for one-step inactivation of chromosomal genes (Datsenko and Wanner, 2000). Briefly, the DNA fragment to be integrated (containing either MS2-PinT or MS2 alone, each fused to the kanamycin resistance cassette in pKD4) was generated via overlapping PCR: the two DNA fragments obtained by PCR with primer pair JVO-16440/16441 or JVO – 16440/16649, respectively, on *Salmonella* gDNA and primer pair JVO-0203/16442 on pKD4 were mixed in equimolar amounts and used as template for a PCR with primer pairs JVO-16443/16444. The chromosomal MS2-PinT or MS2 alone were subsequently transduced to strain JVS-1574, cured with pCP20, resulting in strains JVS-12103 and JVS-12247.

For western blot detection of potential PinT targets, a 3xFLAG epitope sequence was fused to the C terminus of the corresponding protein. To this end, PCR primers (listed in Table S2) each carrying 36-40 nt overhangs homologous to the last portion of the targeted gene (forward primer) and to a region downstream of the stop codon (reverse primer) and *Salmonella* genomic template DNA were

used for PCR amplification. The PCR product was cloned into pSUB11 and transformed into strain JVS-3013. P22 lysates were prepared from positive clones and used to transduce strain YCS-034. Successful insertion was verified by PCR.

All bacterial strains, plasmids and oligonucleotides used in this study are listed in Table S2.

Validation of MS2-PinT expression

To confirm expression of MS2-PinT and compare steady-state levels of the tagged sRNA to wild-type PinT, the strains SCS-001 and JVS-11716 were diluted 1:100 from an overnight culture and grown in LB with 50 μg/mL ampicillin. At OD_{600} of 2.0, expression of tagged or untagged PinT from the plasmid was induced by adding 0.1% of arabinose to the media. After 10 minutes, 4 OD equivalents of cells were collected, mixed with StopMix (Eriksson et al., 2003) and immediately frozen in liquid nitrogen. Total RNA was extracted using TRIzol LS reagent (Invitrogen) according to the manufacturer's recommendations and analyzed by Northern blot, as described below.

Validation of target repression by MS2-PinT

To measure *sopE* and *sopE2* turnover after MS2-tagged or untagged PinT overexpression, strains SCS-001 and JVS-11716 were grown overnight and diluted 1:100 in LB with 50 μg/mL ampicillin. Cultures were grown at 37°C with shaking till they reached OD_{600} of 2.0. Then, 4 OD equivalents of cells were harvested for RNA extraction and the residual cultures kept incubating. Next, 0.1% of arabinose was added to the media in order to induce PinT expression. Total RNA samples were collected at 1, 2, 5 and 10 min after induction, mixed with StopMix and immediately frozen in liquid nitrogen. Total RNA was extracted using TRIzol LS reagent (Invitrogen), as above. RNA samples were treated with DNase I (Fermentas) for 45 min at 37°C. DNase I was then removed using phenol-chloroform extraction and RNA was ethanol-precipitated at −20°C. Efficient removal of genomic DNA was confirmed by PCR using oligonucleotides JVO-1224/1225 (Table S2). Samples were subjected to qRT-PCR measurement, as described below.

Northern blot

As per default, each 5 μg of total RNA were loaded per lane and separated in 6% (vol/vol) polyacrylamide (PAA)-7 M urea gels. RNA was transferred onto Hybond XL membranes (Amersham) by electro-blotting (1 h, 50 V, 4°C) in a tank blotter (Peqlab), crosslinked with UV light and hybridized at 42°C with gene-specific ^{32}P-end-labeled DNA oligonucleotides (Table S2) in Hybri-Quick buffer (Carl Roth AG). After exposure, the screens were read out on a Typhoon FLA 7000 phosphorimager (GE Healthcare).

For the Northern blot experiment with intracellular *Salmonella* (Figure 5A), HeLa-S3 cells were infected with the respective strains (Table S2) at an MOI of 50, as previously described (Westermann et al., 2019). At the indicated time points, host medium was aspirated, the infected cells washed once in PBS and harvested in 500 μL of TRIzol. Each 50 μg/lane were loaded on a 6% PAA-7 M urea gel and blotted as above.

Quantitative real-time PCR (qRT-PCR)

qRT-PCR was performed with the Power SYBR Green RNA-to-CT 1-Step kit (Applied Biosystems) according to the manufacturer's instructions. Fold changes for *pinT*, *sopE*, *sopE2* and *steC* were determined using the $2^{(-\Delta\Delta Ct)}$ method (Livak and Schmittgen, 2001) using 5S rRNA as reference transcript (see Table S2 for qRT-PCR primers).

GFP reporter assay

To measure the GFP intensity of *sopE::gfp*, *steC::gfp*, and *steC*$^{\#}$*::gfp* reporter strains overexpressing MS2-PinT, PinT, or PinT$^{\#}$, the respective strains (see Table S2) were grown in LB or SPI-2-inducing medium (Löber et al., 2006) in presence of ampicillin and chloramphenicol until an OD_{600} of 2.0 (LB) or 0.3 (SPI-2 medium) was reached. *Salmonella* cells corresponding to 1 OD were pelleted and fixed with 4% paraformaldehyde (PFA). GFP fluorescence intensity was quantified for 100,000 events by flow cytometry with the FACSCalibur instrument (BD Biosciences) using a previously described gating strategy (Westermann et al., 2016). Data were analyzed using the Cyflogic software (CyFlo).

In vitro MS2 affinity purification

For the MAPS experiment under the SPI-1 condition (Figure 2A), *Salmonella* strains harboring either MS2-PinT (pYC362; strain SCS-001), or untagged PinT (pYC5-34; strain SCS-002), or the MS2 tag alone (pYC310; strain SCS-039) on a pBAD plasmid were grown in each 10 mL LB supplemented with 50 μg/mL ampicillin (diluted 1:100 from an overnight culture). At OD_{600} of 2.0, overexpression of the different constructs was induced by the addition of 0.1% arabinose. After two minutes, an equivalent of 60 ODs of cells was harvested and chilled on ice for 5 minutes. For MAPS under the SPI-2 condition, the chromosomally MS2-tagged strains (JVS-12103, JVS-12247) were grown overnight in LB medium, the next day washed three times in PBS and diluted 1:50 in 10 mL of SPI-2-inducing minimal medium (Löber et al., 2006). The cultures were grown till they reached an OD_{600} of 0.3 and a 60 OD equivalent was harvested. In each case, cells were then centrifuged at 10,000 g for 10 min and the pellets frozen in liquid nitrogen. After thawing on ice, the pellets were resuspended in 600 μL of chilled Buffer A (20 mM Tris pH 8.0, 150 mM KCl, 1 mM of $MgCl_2$, 1 mM DTT). A volume of 750 μL of glass beads was added to lyse the cells using a Retsch instrument (10 min, 30 Hz; adaptors were pre-chilled at −20°C). The lysates were cleared by centrifugation for 10 min at 16,000 g at 4°C and collected in fresh reaction tubes.

While the lysates were being prepared, affinity purification columns were set up in a 4°C room. ~70 μL of amylose (New England Biolabs) were added to 2 mL Bio-Spin disposable chromatography columns (BioRad). Amylose beads were washed three times with 2 mL of Buffer A. 1 mL of Buffer A with 250 pmol of MS2-MBP coat protein was added to the closed column followed by incubation with rotation at 4°C. After 5 minutes, the column was open and the MS2-coat protein was allowed to run through the column and collected in a separate tube. This incubation step was repeated one more time and thereafter the column was washed once with 1 mL of Buffer A.

The cleared lysates were subjected to affinity chromatography (all steps performed at 4°C). Lysate was added to the closed column and incubated for 5 min with rotation. The flow through was collected and the incubation step was repeated once. Next, the column was washed 8 times with each 2 mL of Buffer A. Bound RNA was eluted using 300 μL of Elution Buffer (Buffer A + 15 mM maltose). This step was repeated one more time. Eluted RNA was extracted with phenol-chloroform and precipitated by the addition of 2 volumes of ethanol and 15 μg of glycogen (1 μL of Glycoblue; 15 mg/mL). RNA samples were treated with DNase I (Fermentas) for 45 min at 37°C. DNase I was then removed using phenol-chloroform extraction and RNA was again ethanol-precipitated.

Salmonella infection assay for *in vivo* MAPS

Immortalized bone marrow-derived macrophages (iBMMs) were infected (MOI 50) with the *Salmonella* strains (strains JVS-11979, JVS-12092, JVS-12093) harboring the respective plasmids (pYC55, pSS31, pSS32) following a previously published protocol (Westermann and Vogel, 2018) with slight modifications. Briefly, two days before infection, 2×10^5 iBMMs/mL were seeded in 10 mL complete DMEM (GIBCO) in T75 flasks (Corning). *Salmonella* overnight cultures were diluted 1:100 in 10 mL of fresh LB medium and grown aerobically to an OD_{600} of 2.0. Bacterial cells were harvested by centrifugation (2 min at 12,000 rpm, room temperature), opsonized in 10% mouse serum for 20 min at room temperature and added to the cells, followed by a 10 min centrifugation step at 250 g, room temperature, to synchronize bacterial uptake. A total of four flasks were infected with each *Salmonella* strain. 30 min afterward, gentamicin-containing DMEM medium (50 μg/mL) was added to eradicate the remaining extracellular bacteria. After 4 h of infection, the medium was aspirated, host cells were washed with ice-cold PBS and lysed with a solution of 0.1% Triton X-100 in PBS. The thus released bacterial cells were separated from host debris by centrifugation at 500 g for 5 min. The supernatant containing the bacterial cells was transferred to a new reaction tube and centrifuged at 10,000 g for 5 min. The bacterial pellet was washed once with PBS and subjected to the MAPS procedure, as described above.

cDNA library preparation and sequencing

The RNA samples were first fragmented using ultrasound (4 pulses of 30 s each at 4°C). Then, an oligonucleotide adaptor was ligated to the 3′ end of the RNA molecules. First-strand cDNA synthesis was performed using M-MLV reverse transcriptase and the 3′ adaptor as primer. First-strand cDNA was purified and 5′ Illumina TruSeq sequencing adapters were ligated to the 3′ end of the antisense cDNA. The resulting cDNA was PCR-amplified (11 cycles) to about 10-20 ng/μL using a high-fidelity DNA polymerase. The cDNA was purified using the Agencourt AMPure XP kit (Beckman Coulter Genomics) and analyzed by capillary electrophoresis. For sequencing, the samples were pooled in approximately equimolar amounts. The cDNA pool in the size range of 200-550 bp was eluted from a preparative agarose gel and sequenced on an Illumina NextSeq 500 system in paired-end mode (2x50, 2x75 or 2x76 cycles, respectively).

MAPS data analysis and target selection

For SPI-1 and SPI-2 data, Illumina reads were quality and adaptor trimmed with Cutadapt (Martin, 2011) using a cutoff Phred score of 20 and reads without any remaining bases were discarded (SPI-1: version 1.10/1.12 with parameters -q 20 -m 1 -a AGATCGGAAGAGCACACGTCTGAACTCCAGTCAC -A AGATCGGAAGAGCGTCGTGTAGGGAAAGAGTGT; SPI-2: version 1.16 with parameters–nextseq-trim = 20 -m 1 -a AGATCGGAAGAGCACACGTCTGAACTCCAGTCAC -A AGATCGGAAGAGCGTCGTGTAGGGAAAGAGTGT). Afterward, we applied the pipeline READemption (Förstner et al., 2014) version 0.4.3 to align all reads longer than 11 nt (-l 12) to the *Salmonella* Typhimurium SL1344 genome (RefSeq assembly accession: GCF_000210855.2) and sequences of the MS2-PinT, MS2 and PinT constructs, respectively, using segemehl version 0.2.0 (Hoffmann et al., 2009) in paired-end mode (-P) with an accuracy cut-off of 95% (-a 95). We used READemption gene_quanti to quantify aligned reads overlapping genomic features by at least 1 nt (-o 1) on the sense strand (-a). For this, we utilized RefSeq annotations (CDS, tRNA, rRNA, transcript) for assembly GCF_000210855.2 complemented with custom annotations for 5′UTRs, 3′UTRs and sRNAs as conducted previously (Holmqvist et al., 2018). Afterward, normalization factors were calculated using the DESeq normalization procedure (Anders and Huber, 2010) on read counts solely for rRNA annotations. Based on these normalization factors and otherwise using default parameters, we conducted differential gene expression analysis of MS2-PinT samples versus PinT/WT and MS2 control samples via DESeq2 (Love et al., 2014) version 1.13.8 for SPI-1 samples (two replicates per condition). For SPI-2 samples (1 replicate per condition) we applied GFOLD (Feng et al., 2012) version 1.1.4 for the comparison also using default parameters except for the pre-calculated size factors. In addition, we utilized READemption to generate coverage plots representing the numbers of mapped reads per nucleotide for visualization in a genome browser again normalizing via the rRNA-based size factors.

For *in vivo* data, Illumina reads were quality and adaptor trimmed with Cutadapt (Martin, 2011) using a cutoff Phred score of 20 and reads without any remaining bases were discarded (version 1.16/2.5 with parameters–nextseq-trim = 20 -m 1 -a AGATCGGAAGAGCACACGTCTGAACTCCAGTCAC -A AGATCGGAAGAGCGTCGTGTAGGGAAAGAGTGT). Afterward, we applied the pipeline

READemption (Förstner et al., 2014) version 0.4.5 to align all reads longer than 19 nt (-l 20) to the *Salmonella* Typhimurium SL1344 (RefSeq assembly accession: GCF_000210855.2) and mouse (GRCm38.p6) genome as well as sequences of the MS2-PinT, MS2 and PinT constructs, respectively, using segemehl version 0.2.0 (Hoffmann et al., 2009) in paired-end mode (-P) with an accuracy cut-off of 90% (-a 90), enabling spliced read detection (-S) and using the re-aligner lack (-r). Read quantification was conducted as described above for SPI-1/2 samples using only *Salmonella* annotations. Afterward, differential gene expression analysis of MS2-PinT versus PinT and MS2 control samples was conducted via DESeq2 (Love et al., 2014) version 1.24.0 using again *Salmonella* rRNA-based size factors for normalization and applying fold-change shrinkage by setting betaPrior = TRUE. We also generated coverage plots via READemption, extracted coverage values for *Salmonella* genome sequences only and again normalized them via rRNA-based size factors.

For the selection of target candidates, we focused on the comparison between MS2-PinT and PinT alone; the MS2-only sample was not used for target selection because we noticed that *bona fide* PinT targets (e.g., *sopE*/*E2* mRNAs) were strongly enriched in the MS2 pull-down itself – probably due to the absence of endogenous *pinT* leading to the de-repression of PinT target transcripts in the input sample. Target candidates were instead selected by considering the log2-fold-change between MS2-PinT versus PinT samples and further filtered by searching for regions with partial complementarity to the previously determined PinT seed region (Westermann et al., 2016) using the IntaRNA software (Busch et al., 2008). In addition, the SalCom database (Kröger et al., 2012; Srikumar et al., 2015) was interrogated, which contains global gene expression data of *Salmonella* Typhimurium under a variety of experimental conditions. Taking into account that PinT is a known virulence-associated sRNA (Kim et al., 2019; Westermann et al., 2016), we prioritized target candidates that are highly expressed under infection-relevant conditions in SalCom.

Time-course pulse expression of PinT under SPI-1 and SPI-2 conditions

To determine the mRNA levels of target candidates in response to PinT, a time-course sRNA pulse expression experiment was performed. Strains harboring the PinT expression plasmid or the empty vector (SCS-002, SCS-013) were grown overnight and diluted 1:100 in LB at 37°C with shaking until OD_{600} of 2.0 was reached and then induced with arabinose, as above. In parallel, the same strains were grown in SPI-2 inducing medium (Löber et al., 2006) to OD_{600} 0.3 and then PinT expression was induced. Bacterial cell samples were collected before or 5, 10 and 20 min after sRNA induction, mixed with StopMix and immediately frozen in liquid nitrogen. Total RNA was extracted using hot phenol, contaminating DNA was removed by DNase I treatment and qRT-PCR was performed as described above.

Western blot

Routinely, protein samples were harvested in 1x sample loading buffer, boiled for 10 min at 95°C and 20 μL/lane were loaded onto a 10% PAA gel for SDS-PAGE. Gel-fractionated proteins were blotted for 90 min (0.2 mA/cm^2; 4°C) in a semi-dry blotter (Peqlab) onto a PVDF membrane (Perkin Elmer) in transfer buffer (25 mM Tris base, 190 mM glycin, 20% methanol). Blocking was for 1 h at room temperature in 10% dry milk/TBST20. Appropriate primary antibodies (see Table S2) were hybridized at 4°C overnight and – following 3× 10 min washing in TBST20 – secondary antibodies (Table S2) for 1 h at room temperature. After three additional washing steps for each 10 min in TBST20, blots were developed using Western Lightning solution (Perkin Elmer) in a Fuji LAS-4000.

For the western blot experiment with intracellular *Salmonella* (Figure 5A), HeLa-S3 cells were infected with the respective strains (Table S2) at an MOI of 50, as previously described (Westermann et al., 2019). At the indicated time points, host medium was aspirated, the infected cells washed once in PBS and harvested in 500 μL of 1x protein loading dye/well. Each 30 μL were loaded per lane of a 10% PAA gel and analyzed as above.

In vitro structure probing and gel mobility shift assays

DNA templates that contain the T7 promoter sequence for *in-vitro* transcription using the MEGAscript T7 Kit (Invitrogen) were generated by PCR. Oligonucleotides and DNA templates used to generate the individual T7 templates are listed in Table S2. Gel-shift assays were performed with ~0.04 pmol 5′ end labeled PinT or *steC* mRNA truncated variant (from TSS to +250 nt). After denaturation (1 min at 95°C), labeled RNAs were chilled for 5 min on ice and 1 μg yeast RNA and 10x RNA structure buffer (Ambion) were added. Increasing concentrations of unlabeled counterpart RNA were added to the indicated final concentrations. After incubation for 1 h at 37°C, samples were immediately supplemented with 3 μL of 5x native loading dye (0.5x TBE, 50% (vol/vol) glycerol, 0.2% (wt/vol) xylene cyanol and 0.2% (wt/vol) bromophenol blue) and loaded on a native 6% (vol/vol) PAA gel. For gel-shifts with Hfq, ~0.04 pmol 5′ end labeled PinT were incubated with increasing concentrations of unlabeled *steC* to final concentrations of 12 nM, 94 nM, 375 nM, 750 nM, 1,500 nM and 3,000 nM. Upon addition of purified Hfq (250 nM) or Hfq dilution buffer (negative control), samples were incubated at 37°C for 1 h. Gel electrophoresis was performed in 0.5x TBE buffer at 300 V. Gels were dried and analyzed using a PhosphoImager (FLA-3000 Series, Fuji) and the ImageJ software (NIH).

Secondary structure probing and mapping of RNA complexes were conducted with 5′ end-labeled RNA (~0.1 pmol) in 10 μL reactions. RNA was denatured for 1 min at 95°C and chilled on ice for 5 min, upon which 1 μg of yeast RNA and 10 × structure buffer (0.1 M Tris at pH 7, 1 M KCl, 0.1 M $MgCl_2$; Ambion) were added. The concentrations of unlabeled sRNA/mRNA leader added to the reactions are given in the respective figure legend. Following incubation for 1 h at 37°C, 2 μL of lead(II) acetate (25 mM; Fluka), or 2 μL of RNase T1 (0.01 U/μL; Ambion) were added and incubated for 45 s, 3 min, or 10 min at 37°C, respectively. RNase III cleavage reactions (Shortcut RNase III; 0.02 U/μL; NEB) contained 1 mM DTT and 1.3 U of enzyme, and were incubated for 6 min at 37°C.

Reactions were stopped with 12 μL of loading buffer on ice. RNase T1 ladders were obtained by incubating labeled RNA (~0.2 pmol) in 1 × sequencing buffer (Ambion) for 1 min at 95°C. Subsequently, 1 μL of RNase T1 (0.1 U/μL) was added, and incubation was continued for 5 min at 37°C. OH ladders were generated by incubating 0.2 pmol of labeled RNA for 5 min in alkaline hydrolysis buffer (Ambion) at 95°C. Reactions were stopped with 12 μL of loading buffer on ice. Samples were denatured for 3 min at 95°C prior to separation on 6% PAA/7 M urea sequencing gels in 1 × TBE. Gels were dried and analyzed using a PhosphorImager (FLA-3000 Series; Fuji) and AIDA software.

In vitro translation assay

Translation reactions were carried out using the PURExpress (New England Biolabs) according to the manufacturer's instructions. In brief, 1 pmol *in vitro* transcribed mRNA (*steC*::*gfp*, *hupA*::*gfp*) was denatured in absence or presence of 50 or 100 pmol of PinT RNA for 1 min at 95°C and chilled for 5 min on ice. Hfq (250 nM) was mixed with mRNA (and sRNA) and preincubated for 10 min at 37°C before addition of PURExpress mix. Translation was performed in a 10 μL reaction for 1 h at 37°C, and stopped with four volumes of ice-cold acetone and chilled on ice for 15 min. Reactions were stopped by addition of 60 μL acetone, chilled for 15 min on ice and proteins were collected by centrifugation for 10 min at 10,000 g and 4°C. *In vitro* translated SteC::GFP or HupA::GFP were quantified by western blot analysis using monoclonal anti-GFP (Roche Applied Science) and anti-mouse IgG (GE-Healthcare) antibodies. The ribosomal protein S1 served as a loading control and was detected by an S1 antibody, (1:10,000, kindly provided by M. Springer, IBPC Paris, France) and anti-rabbit secondary antibody (Thermo Scientific).

Toeprinting assay

Toeprinting reactions were carried out as described (Hartz et al., 1988) with a few modifications. 0.2 pmol of an unlabelled *stec* mRNA fragment (845 nt, T7 template amplified with JVO-15723/PZE-XbaI), and 0.5 pmol of 5′end labeled primer JVO- 1976 complementary to the *gfp* coding region were annealed. For inhibition analysis, 1 and 2 pmol of PinT sRNA were added. Nucleic acids were denatured in annealing buffer (10 mM Tris-acetate pH 7.6, 1 mM DTT, 100 mM potassium acetate) for 1 min at 95°C and chilled on ice for 5 min, upon which Mg^{2+} acetate and all dNTPs were added to final concentrations of 0.5 mM. All subsequent incubation steps were at 37°C. After 5 min incubation, 2 pmol of 30S ribosomal subunit (provided by K. Nierhaus, Max Planck Institute for Molecular Genetics, Berlin, Germany; pre-activated for 20 min prior to the assay) were added. Following incubation for 5 min, uncharged tRNAfMet (10 pmol) was added, and incubations continued for 15 min. Reverse transcription was carried out by addition of 100 U of Superscript II and incubation for 20 min. cDNA synthesis was terminated with 100 μL stop buffer (50 mM Tris-HCl pH 7.5, 0.1% SDS 10 mM EDTA). Following phenol-chloroform extraction, alkaline hydrolysis of template RNA at 90°C, and ethanol precipitation, cDNA was dissolved in 10 μL of loading buffer II (Ambion). Sequencing ladders were generated with CycleReader™ DNA Sequencing Kit (Fermentas) according to the manufacturer's protocol on the same DNA template as used for T7 transcription and the same 5′-end-labeled primer as in the toeprinting reactions. cDNAs and sequence ladders were separated on a 6% PAA/ 7M urea gel. Autoradiograms of dried gels were obtained as above.

Immunofluorescence and confocal microscopy

Immunofluorescence of *Salmonella*-infected Swiss 3T3 cells was performed as previously described (Poh et al., 2008). In summary, one day prior to infection, Swiss 3T3 cells were seeded on 10 mm coverslips at a density of $5x10^4$ cell per well. The next day, infections were carried out as mentioned above, using an MOI of 100. Bacterial uptake was synchronizes by a 10 min centrifugation step at 170 g, room temperature. Cells were allowed to adhere for 30 min. Afterward, gentamicin-containing DMEM medium (100 μg/mL) was added to eradicate the remaining extracellular bacteria. After 1 h, the medium was replaced by DMEM medium containing 16 μg/mL of gentamycin. At 10 h p.i. the coverslips were washed with PBS (GIBCO) and fixed in 4% (w/v) PFA for 15 min in the dark. After three additional PBS washing steps, cells were stained with Alexa Fluor 594 Phalloidin (ThermoFisher; 1:250 diluted in PBS) for 15 min in the dark and again washed twice with PBS. After coverslips had been air-dried, they were embedded in VECTASHIELD(R) Mounting Medium (Biozol) with DAPI and analyzed using the LEICA SP5 confocal microscope (Leica) and the LAS AF Lite software (Leica).

QUANTIFICATION AND STATISTICAL ANALYSIS

Quantification of band intensities in Figure 5A was performed using the ImageJ software (NIH). Where applicable, statistical significance was calculated using the Fisher's exact test, with the statistical details and biological replicates of the experiments to be found in the corresponding figure legends.